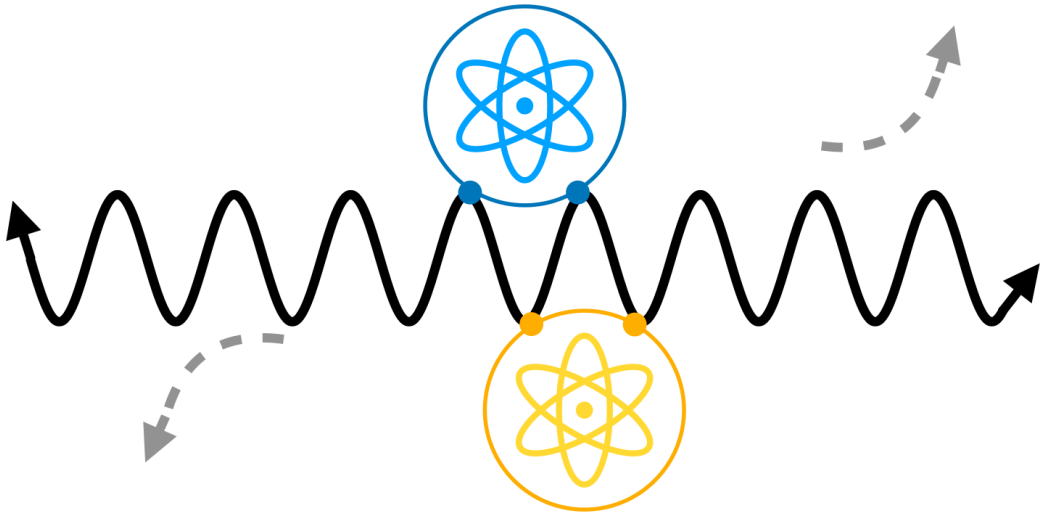

Quantum Optics with Giant Atoms in Imperfect Waveguides

Master's Thesis in Microtechnology and Nanoscience

JINGYI ZHOU

DEPARTMENT OF MICROTECHNOLOGY AND NANOSCIENCE

CHALMERS UNIVERSITY OF TECHNOLOGY
Gothenburg, Sweden 2026
www.chalmers.se

Master's thesis 2026

Quantum Optics with Giant Atoms in Imperfect Waveguides

JINGYI ZHOU

CHALMERS
UNIVERSITY OF TECHNOLOGY

Department of Microtechnology and Nanoscience
Chalmers University of Technology
Gothenburg, Sweden 2026

Quantum Optics with Giant Atoms in Imperfect Waveguides

Jingyi Zhou

Supervisor: Anton Frisk Kockum, Department of Microtechnology and Nanoscience
Examiner: Anton Frisk Kockum, Department of Microtechnology and Nanoscience

Master's Thesis MCCX60
Department of Microtechnology and Nanoscience
Chalmers University of Technology
SE-412 96 Gothenburg
Telephone +46 31 772 1000

Cover: Illustration of two giant atoms in a braided configuration coupled to a lossy waveguide.

Typeset in LaTeX
Gothenburg, Sweden 2026

Quantum Optics with Giant Atoms in Imperfect Waveguides

Jingyi Zhou
Department of Microtechnology and Nanoscience
Chalmers University of Technology

Abstract

The rapid advancement of quantum technologies has driven the exploration of novel regimes in quantum light-matter interactions to overcome fundamental limits in coherence and control. Giant atoms, characterized by their ability to couple to a waveguide at multiple points separated by distances comparable to the wavelength of the guided light, have emerged as a promising platform for quantum optics. The phase shifts accumulated by photons traveling between these coupling points give rise to both self-interference and collective interference effects. Self-interference allows a single giant atom to decouple from its environment, preventing relaxation into the waveguide. For multiple giant atoms, the interference effects provide two mechanisms for decoherence suppression: the formation of *dark states* in driven and undriven systems and *decoherence-free interaction* (DFI) in a certain configuration. Previous studies in this emerging field have assumed the waveguide to be lossless. In this thesis, we investigate the impact of two realistic imperfections: losses in the waveguide and asymmetric coupling, where the relaxation rates at each coupling point are unequal. Utilizing the *SLH formalism* for cascaded quantum systems, we derive the *Lindblad master equation* to model the dynamics of the system. Through numerical simulations, we quantify the extent to which these imperfections influence giant-atom phenomena. Our results determine the upper bounds of losses per distance in recent experiments and also the tolerances of losses in forming a highly entangled state. The results presented in the report introduce essential, realistic considerations for topology designs and driven configurations in future giant-atom experiments, laying the foundation for realizing implementations in quantum technologies.

Keywords: quantum optics, giant atoms, losses, waveguides, decoherence-free interaction, frequency-dependent relaxation rate, SLH formalism, dark states.

Acknowledgements

For the completing of this thesis, I would like to first express my sincere gratitude to my supervisor Anton Frisk Kockum for providing a lot of professional suggestions and support during the entire thesis project. Before this project, "giant atoms" was a completely unfamiliar field to me. It is a very good one-year research journey to discuss and work with Anton, and I have made progress in the process of completing this thesis. I also want to thank the Wallenberg Centre for Quantum Technology, as well as the Marianne and Marcus Wallenberg foundation for supporting my whole master's study. In addition, I want to thank Lei Du and Jingjun Zhu for many helpful discussions when I faced difficulties in the study. I would also like to thank all members of the giant atoms team for creating a welcoming and inspiring atmosphere. Finally, I want to give my gratitude to my family and friends for their listening, encouragement and companionship, whether near or far.

Jingyi Zhou, Gothenburg, June 2026

List of Acronyms

DFI	Decoherence-free interaction
SAW	Surface acoustic waves
RWA	Rotating-wave approximation
H.c.	Hermitian conjugate

Nomenclature

r	Atom radius
λ	Wavelength
ϕ	Phase shift between neighboring coupling points
d	Distance between neighboring coupling points
k	Wave number
$\|\psi\rangle$, $\|\psi_\alpha\rangle$	System state
H	Hamiltonian
ρ	Density matrix
c_α	Possibility of the specific system state
$\mathcal{L}$	Liouville super-operator
X	Any operators
γ, Γ	Relaxation rate
$\mathcal{D}[X]\rho$	Dissipator
L	Jump operator
ω_j	Atom frequencies ($j = a, b$)
σ_z	Pauli matrix
$a(a^\dagger)$	Annihilation (creation) operator
ω_k	Frequency of each bath mode
g	Coupling strength between the atom and the bath
$\sigma_\pm$	Ladder operators
U	Unitary time evolution operator
t, τ	Time
ω_j'	Lamb-shifted transition frequency
δ_{ω_j}	Lamb shift
J_ω	Bath state density
$\|e\rangle$, $\|g\rangle$	Excited and ground state

G	SLH triplet
$\mathbf{S}$	Scattering matrix
$\mathbf{L}$	Coupling vector
$\gamma_{nR/L}$	Left-/right-directed relaxation rate at point n
γ_n	Bare relaxation rate at point n $\gamma_{nR} + \gamma_{nL} = \gamma_n$
d	Distance between neighboring coupling points
Γ_j	Effective/individual relaxation rate ($j = a, b$)
Γ_{coll}	Collective relaxation rate
g	Exchange interaction
$\lvert D\rangle$, $\left\lvert D_{S/T}\right\rangle$	Dark state
E	Eigenvalue
$\mathbb{R}$	set of real numbers
$\lvert S/T\rangle$	Singlet/triplet state
β	Complex amplitude of a coherent drive
α	Probability amplitude
Δ_γ	Difference between the left- and right-directed relaxation rates $\gamma_L - \gamma_R$
δ_j	Detuning of the atomic frequency from the drive
r, t	Reflection and transmission coefficients
ε	Total losses between neighboring coupling points
f	Attenuation coefficient
ϵ	Ratio of the bare relaxation rates belonging to the same atom γ_1/γ_2
δ_{Γ_j}	Vertical shift of the minimum individual relaxation rate
δ_d	Horizontal shift of the distance corresponding to the minimum individual relaxation rate

Contents

List of Figures

List of Tables

1

Introduction

The second quantum revolution, which mainly focuses on harnessing the complex quantum phenomena such as entanglement and superposition, is currently driving the development of quantum technologies, including quantum computing and quantum simulation. These approaches can solve problems that are intractable on classical computers more efficiently [1].

Quantum optics, which studies light-matter interaction on a quantum scale, is important in the development of quantum computing and simulation. In quantum optics, the concepts of superposition and entanglement form the theoretical foundation for quantum computers [2]. Recently, a new type of quantum emitter has emerged—*giant atoms* [3], which can couple to light at multiple separated points that are wavelength distance apart. In the following, we introduce the background and the key properties of giant atoms, and conclude the chapter by outlining the scope and structure of this thesis.

1.1 Small and giant atoms

Traditionally, quantum optics has focused on natural atoms, which are very small (radius $r \approx 10^{-10}$ m) compared with the wavelength of optical light ($\lambda \approx 10^{-6}$–10^{-8} m) [3]. Thus, the coupling point can be approximated as a pointlike to simplify the description of the light-matter interaction (Fig. 1.4a) [3].

In contrast, *giant atoms* can be engineered in platforms such as superconducting circuits [4], which have some properties of natural atoms, such as discrete energy levels, the ability to emit and absorb single photons, and non-linear response. Although the physical size of superconducting qubits ($r \approx 10^{-4}$–10^{-3} m) is still less than the wavelength of the microwave field ($\lambda \approx 10^{-2}$–10^{-1} m) they interact with [3], they can couple to the field at multiple different points (Fig. 1.4b) by meandering a waveguide for the microwaves on the chip (Fig. 1.1a, 1.2b). Consequently, their effective size can be comparable to the field wavelength (hence their name).

Waves emitted from different coupling points acquire propagation-induced phase differences, introducing interference effects. Interference between coupling points leads to *frequency-dependent relaxation rates* (Fig. 1.1c) [7], as the phase shifts depend on the distance between coupling points and the wave frequency, i.e., $\phi = kd$, where k is the wave number. This property makes giant atoms can be engineered by

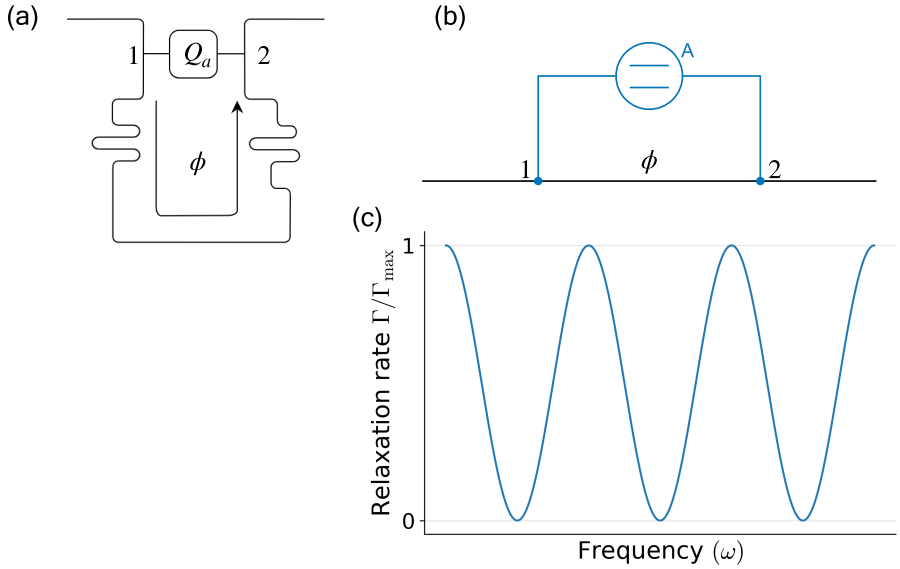

Figure 1.1: (a) A single giant atom coupled to a meandering waveguide. Figure adapted from Ref. [5]. (b) A giant atom coupled to a waveguide at two separated points. Figure adapted from Ref. [6]. (c) Frequency dependence of the relaxation rate for a single giant atom.

tuning the atomic transmission frequency and distance between coupling points [7].

Another noteworthy phenomenon of giant atoms is *decoherence-free interaction* [8]. Specifically, in a braided configuration with two (Fig. 1.2a) or more giant atoms, where their coupling points are interleaved along the waveguide, the atoms can coherently interact with each other via the waveguide, while each remains effectively decoupled from the waveguide, thereby suppressing decoherence [8], as illustrated by Fig. 1.2c. This property can be used to achieve a scalable and tunable quantum simulator for open quantum systems [9]. Tuning the system to decoherence-free points enables the implementation of a universal gate set of single- and two-qubit gates, which enables the simulation of coherent (closed system) dynamics, while tuning to points with decoherence allows the simulation of losses characteristic of open quantum systems.

Besides decoherence-free interaction, there is also a less robust way to protect the system from decoherence: *dark states* (shown in Fig. 1.3). In many-atom systems, states that exhibit a slower decay than the relaxation of each individual atom are characterized as *subradiant states* [10–13]. A dark state represents a perfectly subradiant state and can be realized in both undriven and driven systems. In undriven systems, two atoms can share a single excitation in a collective superposition, where spontaneous emission is suppressed through destructive interference [14]. In the driven-dissipative regime, this two-atom system evolves toward a dynamic equilibrium between external drive and scattering, where bosonic streams scattered from different atoms interfere destructively [14].

The dark state is instrumental for efficient energy transfer and decoherence sup-

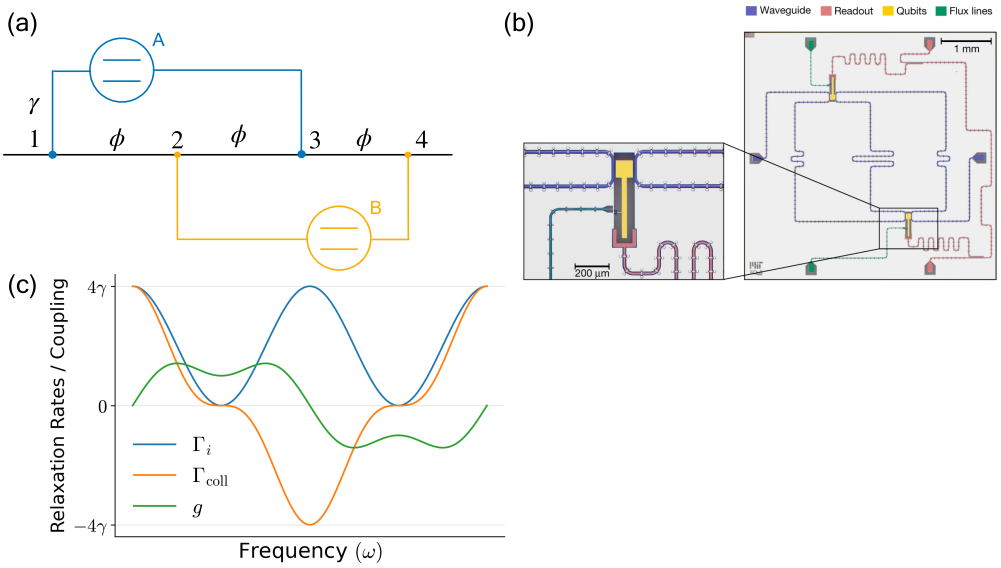

Figure 1.2: (a) A braided-atom system. Figure adapted from Ref. [6]. (b) A false-color optical micrograph image of the chip in the braided configuration. Figure reproduced from Ref. [5]. (c) Frequency dependence of relaxation rates (blue and orange lines) and coherent coupling (green line) for braided atoms. There is the same atomic frequency and the same distance between neighboring coupling points.

pression [13, 14, 16]. Giant atoms, characterized by their highly tailorable and reconfigurable properties, offer a potential platform to generate dark states. This is important for quantum communication, which aims to transfer a quantum state from one place to another [17]. Additionally, the distance-introduced interference, quantum coherence and entanglement in giant atoms can be leveraged to improve the sensitivity and precision of quantum sensors [18].

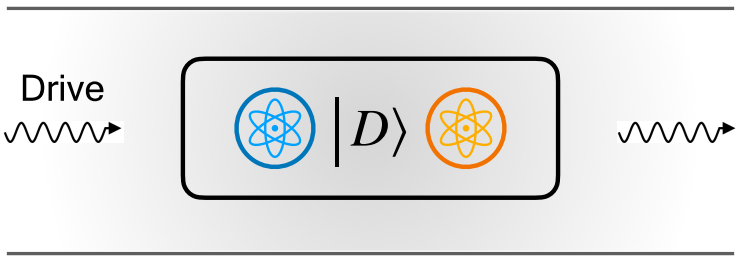

Figure 1.3: Two atoms coupled to a waveguide form a dark state. For entire two-atom systems (the small rounded rectangle), there is no emission or absorption of photons. Therefore, the drive from the left side of the waveguide can be fully transmitted through the system. Figure inspired by Refs. [14, 15].

1.2 Aims, scope and outline

To date, most theoretical studies on giant atoms have assumed ideal waveguides, since waveguides used in the relevant experiments have quite low losses per distance, such as superconducting transmon qubit coupled to surface acoustic waves (SAW) [19] and superconducting qubit coupled to superconducting waveguides [5]. However, in practice, experimental environments are inherently imperfect. As we want to push toward highly sophisticated experiments and high-performance applications in quantum technologies, it becomes important to understand the impact of imperfections on giant-atom platforms and to identify the thresholds at which impact becomes noticeable.

This thesis focuses on two specific types of imperfections: losses in the waveguide (Fig. 1.4c) and the asymmetric coupling of giant atoms, where the giant atom exhibits disparate relaxation rates at its multiple coupling points. The primary goal of this study is to establish a quantitative performance border for giant atom systems under such imperfect conditions, thereby providing practical guidelines for engineering setups in experiments.

To achieve this, we explore how the behavior of giant atoms is influenced by these imperfections. We combine the analytical solutions of the relaxation rates with the experimental data to determine the upper bound of losses. By comparing the shifts *decoherence-free point* with the maximum relaxation rates, we demonstrate this extremely low losses. In addition, we analyze the shifts of the *decoherence-free point* caused by losses versus asymmetry to distinguish between these two imperfections. A limitation of the thesis is that for more complicated setups, such as two atoms coupled to a waveguide, we do not simultaneously account for waveguide losses and asymmetric coupling. Regarding dark states, we investigate both driven and undriven systems, employing numerical simulation to determine the system's tolerance to losses.

The structure of this thesis is as follows. In Chapter 2, we introduce the theoretical tools used in modeling atoms coupled to a waveguide. For clarity, detailed examples are shown in some sections: a single giant atom and a system of two giant atoms. Subsequently, we extend our analysis to lossy waveguides. In Chapter 3, we present and discuss the results obtained using the methodology developed in the previous chapter, addressing the key questions raised above. Finally, Chapter 4 provides a summary of our findings and offers an outlook.

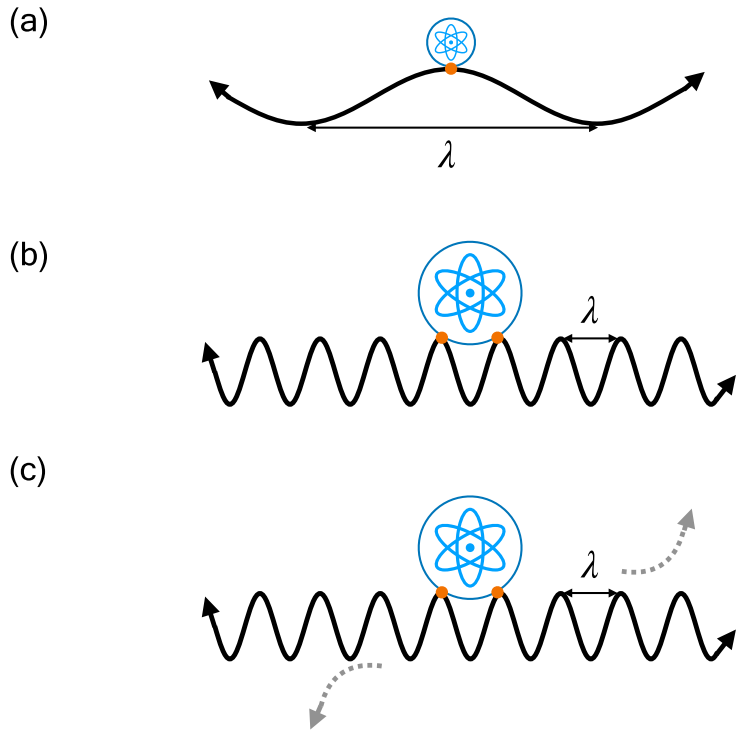

Figure 1.4: (a) A small atom coupled to a waveguide supporting a field with wavelength λ. Figure adapted from Ref. [5]. (b) A giant atom coupled to a waveguide at two separated points, interacting with a field of wavelength λ. Figure adapted from Ref. [5]. (c) A giant atom coupled to a lossy waveguide at two separated points, interacting with a field of wavelength λ.

2

Theory

In this chapter, we introduce the background knowledge required to model giant atoms coupled to a waveguide, which is necessary for a full understanding of the discussions and results presented in the thesis. We first review the fundamentals of *open quantum systems*, followed by an introduction to the *SLH formalism* for cascaded quantum systems. Several examples are then provided to illustrate how the SLH formalism is applied to model giant-atom systems. Finally, building on this foundation, we show how giant atoms in a lossy waveguide can be modeled.

2.1 Quantum master equations

When atoms interact with continuous waveguides, the quantum dynamics of atoms change as a consequence of its internal dynamics and of the interaction with the waveguides. Therefore, we consider it as an open quantum system, i.e., a quantum system coupled to a surrounding environment, commonly referred to as a bath. The master equation for the reduced density matrix of the system allows us to focus on how the system dynamics are influenced by the environment, without having to explicitly model the many degrees of freedom in the environment. In order to overcome the obstacle that the environment is composed of infinitely many quantum systems, we make some approximations, which are discussed in the later content.

2.1.1 Closed and open quantum system

First, we present a brief review of master equations (we set $\hbar = 1$ throughout the thesis).

For *closed quantum systems*, in the *Schrödinger picture*, the state of the system $|\psi\rangle$ evolves in time according to the *Schrödinger equation* [20],

$$i\frac{\mathrm{d}}{\mathrm{d}t}|\psi(t)\rangle = H(t)\,|\psi(t)\rangle, \tag{2.1}$$

where $H(t)$ is the Hamiltonian of the system.

Generally, the quantum state ensemble can be characterized by the density matrix [20],

$$\rho = \sum_{\alpha} c_\alpha \,|\psi_\alpha\rangle\,\langle\psi_\alpha|\,, \tag{2.2}$$

where c_α is the probability of the system being in $|\psi_\alpha\rangle$ state. What is more, the probabilities add up to 1, which means that $\mathrm{Tr}\rho = \sum_\alpha c_\alpha = 1$. An important property of the probability is that $\mathrm{Tr}\rho^2 \leq \mathrm{Tr}\rho = 1$, when it holds equality sign, the density matrix has the form $\rho = |\psi\rangle\langle\psi|$ considered as the pure state. In the case of inequality sign, the state is said to be in the mixed state. Here, we consider a general case of mixed state. From the Schrödinger equation, the time dependence of the density matrix is governed by the *Liouville-von Neumann equation* (also referred to as the *von Neumann equation*) [20],

$$\frac{\mathrm{d}\rho(t)}{\mathrm{d}t} = -i[H(t), \rho(t)] = \mathcal{L}\rho, \tag{2.3}$$

which is also the equation of motion for the density matrix. Here, $\mathcal{L}$ is the *Liouville super-operator*. The last equality in the Eq. (2.3) shows an analogy to the classical Liouville equation [20].

For *open quantum systems*, the total Hamiltonian H_{tot} is the sum of the open system self-Hamiltonian H_S, the bath Hamiltonian H_B, and the interaction Hamiltonian H_I,

$$H_{\mathrm{tot}} = H_S + H_B + H_I, \tag{2.4}$$

The reduced density matrix is obtained by tracing out the degrees of freedom of the bath,

$$\frac{\mathrm{d}\rho(t)}{\mathrm{d}t} = -i\mathrm{Tr}_B[H_{\mathrm{tot}}(t), \rho_{\mathrm{tot}}(t)], \tag{2.5}$$

where ρ_{tot} represent the density matrix of the total system (including the bath). In this project, we consider Markov processes, for which the Liouville super-operator $\mathcal{L}$, is defined by,

$$\mathcal{L}\rho = -i[H, \rho] + \sum_k \gamma_k (X_k \rho X_k^\dagger - \frac{1}{2} X_k^\dagger X_k \rho - \frac{1}{2} \rho X_k^\dagger X_k), \tag{2.6}$$

where γ_k play the role of relaxation rates [20]. For convenience, we introduce the dissipator $\mathcal{D}[X]\rho = X\rho X^\dagger - \frac{1}{2}\left\{X^\dagger X, \rho\right\}$, and the *Lindblad master equation* in the form

$$\frac{\mathrm{d}}{\mathrm{d}t}\rho = -i[H, \rho] + \sum_k \gamma_k \mathcal{D}[L_k]\rho, \tag{2.7}$$

the L_k are jump operators [21], representing the different dissipative processes.

2.1.2 Master equation for a single atom coupled to the bath

To illustrate the derivation of a master equation, we consider a model where a single atom couples to a bath of infinitely many harmonic oscillators, such as a waveguide. For simplicity, the atom is a two-level system. Then the total Hamiltonian H_{tot} can be obtained from Eq. (2.4):

$$H_{\mathrm{tot}} = H_a + H_B + H_I, \tag{2.8}$$

$$H_a = \frac{\omega_a}{2}\sigma_z, \tag{2.9}$$

$$H_B = \sum_k \omega_k a_k^\dagger a_k, \tag{2.10}$$

$$H_I = \sum_k g_k(a_k + a_k^\dagger)(\sigma_- + \sigma_+), \tag{2.11}$$

where ω_a is the transition frequency of the atom; σ_z is the Pauli-Z matrix, for the atom, which is usually defined as $\sigma_z = |e\rangle\langle e| - |g\rangle\langle g|$ in the basis $\{|e\rangle, |g\rangle\}$; ω_k is the frequency of each mode; a_k ($a_k^\dagger$) is the annihilation (creation) operator; g_k represent the coupling strength between the atom and the bath; $\sigma_+ = |e\rangle\langle g|$ and $\sigma_- = |g\rangle\langle e|$ are the ladder operators of the atom.

Since the total system (atom plus bath) is closed, its von Neumann equation follows the Eq. (2.3),

$$\frac{\mathrm{d}\rho_{\mathrm{tot}}}{\mathrm{d}t} = -i[H_{\mathrm{tot}}, \rho_{\mathrm{tot}}], \tag{2.12}$$

where H_{tot} is the total Hamiltonian (Eq. (2.3)).

Then we move to *interaction picture* to remove the free evolution ($H_a + H_B$), which is independent of time. This is also to separate the slow dynamics introduced by the interaction between the atom and bath. We first introduce the unitary time evolution operator,

$$U_0(t) = e^{-i(H_a+H_B)t}, \tag{2.13}$$

$$U_I(t) = U_0^\dagger(t)U(t), \tag{2.14}$$

where $U(t)$ is the unitary time evolution operator of the total system i.e., $|\psi(t)\rangle = U(t, t_0)|\psi(t_0)\rangle$, and the initial time t_0 is 0.

Then the interaction picture operators A_I,

$$X_I(t) = U_0^\dagger(t)X(t)U_0(t), \tag{2.15}$$

The interaction density matrix $\rho_I(t)$,

$$\rho_I(t) = U_I(t)\rho(0)U_I^\dagger(t) = U_0^\dagger(t)\rho(t)U_0(t), \tag{2.16}$$

in Eq. (2.16), ρ is the density matrix of the total system (atom plus bath) in Schrödinger picture.

To simplify, the sign $\sim$ is served to indicate the interaction picture, thus von Neumann equation of the total system in form

$$\dot{\tilde{\rho}}_{tot}(t) = -i[\tilde{H}_I(t), \tilde{\rho}_{tot}(t)], \tag{2.17}$$

the integral form of which is

$$\tilde{\rho}_{\mathrm{tot}}(t) = \tilde{\rho}_{\mathrm{tot}}(0) - i\int_0^t \mathrm{d}\tau[\tilde{H}_I(\tau), \tilde{\rho}_{\mathrm{tot}}(t)], \tag{2.18}$$

where τ accounts for the contribution of the interaction Hamiltonian at all past times to the state at present. After substituting Eq. (2.18) back to Eq. (2.17), and tracing out the bath degree of freedom (Eq. (2.5)), we find,

$$\dot{\tilde{\rho}}_a(t) = \mathrm{Tr}_B(-i[\tilde{H}_I(t), \tilde{\rho}_{\mathrm{tot}}(0)] - \int_0^t \mathrm{d}\tau[\tilde{H}_I(t), [\tilde{H}_I(\tau), \tilde{\rho}_{\mathrm{tot}}(\tau)]]). \tag{2.19}$$

This is the equation for the atom density matrix ρ_a. In the right side of Eq. (2.19), the density matrix of the total system ρ_{tot} is still contained. In order to eliminate the ρ_{tot}, we introduce some approximations.

The first key approximation is the *Born approximation*, which states that the coupling g_j between the atom and the bath is weak and that the bath is much larger than the system. Thus, the atom has little impact on the bath, so the density matrix of the bath ρ_B remains approximately unchanged during the evolution. We further assume that, at the initial time t_0, the atom and the bath are uncorrelated. Under weak coupling, the correlations generated during the evolution still remain small, such that the total system state at later times can be characterized by $\tilde{\rho}_{tot}(t) \approx \tilde{\rho}_a(t) \otimes \tilde{\rho}_B(0)$. In addition, for a bath in an equilibrium state, the linear bath operators (a_k and $a_k^\dagger$) in the interaction Hamiltonian have zero expectation value, so that the average contribution of the interaction from the bath vanishes, i.e., $\langle H_I \rangle_B = \mathrm{Tr}_B(H_I \rho_B) = 0$. Then Eq. (2.19) becomes

$$\dot{\tilde{\rho}}_a(t) = -\int_0^t \mathrm{d}\tau \mathrm{Tr}_B[\tilde{H}_I(t), [\tilde{H}_I(\tau), \tilde{\rho}_a(\tau)\tilde{\rho}_B(0)]]. \tag{2.20}$$

The *Markovian approximation* assumes that the bath has no memory, which is justified by the weak interaction between the system and the large number of degrees of freedom in the bath. As a result, any imprint that the atom makes on the bath does not feed back into the system dynamics at later times. Therefore, we can replace $\tilde{\rho}_a(\tau)$ with $\tilde{\rho}_a(t)$ in Eq.(2.20),

$$\dot{\tilde{\rho}}_a(t) = -\int_0^t \mathrm{d}\tau \mathrm{Tr}_B[\tilde{H}_I(t), [\tilde{H}_I(\tau), \tilde{\rho}_a(t)\tilde{\rho}_B(0)]]. \tag{2.21}$$

The approximations above are also referred as *Born-Markov approximation* [20]. The remaining derivation is tracing over the bath, and the details of this calculation are shown in Ref [22]. In this process, the *rotating-wave approximation* (RWA) is applied. In the interaction picture, the interaction Hamiltonian has terms with $a\sigma_-$ and $a^\dagger\sigma_+$, whose oscillation frequency is $\omega_a + \omega_B$. These terms with fast oscillation frequencies are neglected provided that coupling strength is much small than $\omega_a + \omega_B$, while terms with $\omega_a - \omega_B$ are kept [23]. After the bath is traced out, we can transform back from the interaction picture, the final result of the Lindblad master equation is

$$\dot{\rho}_a(t) = -i[\frac{\omega_a'}{2}\sigma_z, \rho_a] + \Gamma\mathcal{D}[\sigma_-]\rho_a, \tag{2.22}$$

where $\omega_a' = \omega_a + \delta_{\omega_a}$ is the Lamb-shifted transition frequency [7, 22], and Γ is the relaxation rate in the form:

$$\Gamma = 2\pi J(\omega_a) g^2(\omega_a), \tag{2.23}$$

where $J(\omega)$ is the bath density of states and $g(\omega_j) = g_j$ is the coupling strength. For this two-level atom, this kind of relaxation transfers the atom from the excited state $|e\rangle$ to the ground state $|g\rangle$ at the rate Γ.

One thing should be noted is that if we want to obtain the exact value of the frequency shift, we cannot apply the RWA too early, i.e., on the interaction Hamiltonian (Eq. (2.11)). Otherwise, the term about the shift of the ground state of the atom in the Lamb shift will be missing [24].

2.2 SLH formalism

Since giant atoms coupled to the waveguide with multiple coupling points is a more complicated system, we use the SLH formalism [25, 26] as a modular framework to model the *cascaded quantum system* [27, 28], where the output from one component is the input to another. This formalism can be used to derive the master equation for the system, which describes the system dynamics under environmental influence. The SLH formalism was initially developed for modeling quantum optical networks called *quantum input-output networks*, in which localized components interact through itinerant bosonic fields [25].

In the SLH formalism, the individual quantum components are specified by triplets $G = (\mathbf{S}, \mathbf{L}, H)$ to capture how the components interact with input and output fields at the input-output ports. Here $\mathbf{S}$ is an $n \times n$ scattering matrix describing scattering among multiple channels [26], $\mathbf{L}$ is an $n \times 1$ vector representing the coupling between the system and the bath, and H is the system Hamiltonian.

2.2.1 SLH rules

In order to construct large networks in many ways, three operations (shown in Fig. 2.1) are defined: the *series product*, the *concatenation product*, and the *feedback* operation.

The series product is denoted by $\triangleleft$ and describes the cascading of the output from one localized component $G_1 = (\mathbf{S}_1, \mathbf{L}_1, H_1)$ into the input of another $G_2 = (\mathbf{S}_2, \mathbf{L}_2, H_2)$. The series product is given by

$$G_2 \triangleleft G_1 = \left(\mathbf{S}_2\mathbf{S}_1, \mathbf{S}_2\mathbf{L}_1 + \mathbf{L}_2, H_1 + H_2 + \frac{1}{2i}(\mathbf{L}_2^\dagger \mathbf{S}_2 \mathbf{L}_1 - \mathbf{L}_1^\dagger \mathbf{S}_2^\dagger \mathbf{L}_2)\right). \tag{2.24}$$

Through input-output theory and quantum stochastic calculus, we get the result that the system performs as if it had a Hamiltonian $H = H_1 + H_2 + (\mathbf{L}_2^\dagger \mathbf{S}_2 \mathbf{L}_1 - \mathbf{L}_1^\dagger \mathbf{S}_2^\dagger \mathbf{L}_2)/(2i)$ and was coupled to the environment through an operator $\mathbf{L} = \mathbf{S}_2\mathbf{L}_1 + \mathbf{L}_2$ [22, 25, 29]. It should be noted that $G_2 \triangleleft G_1 \neq G_1 \triangleleft G_2$ due to the directional coupling between the localized components.

The concatenation product, denoted by $\boxplus$, is used to describe the parallel combination of components. Here, two components $G_1 = (\mathbf{S}_1, \mathbf{L}_1, H_1)$ and $G_2 = (\mathbf{S}_2, \mathbf{L}_2, H_2)$

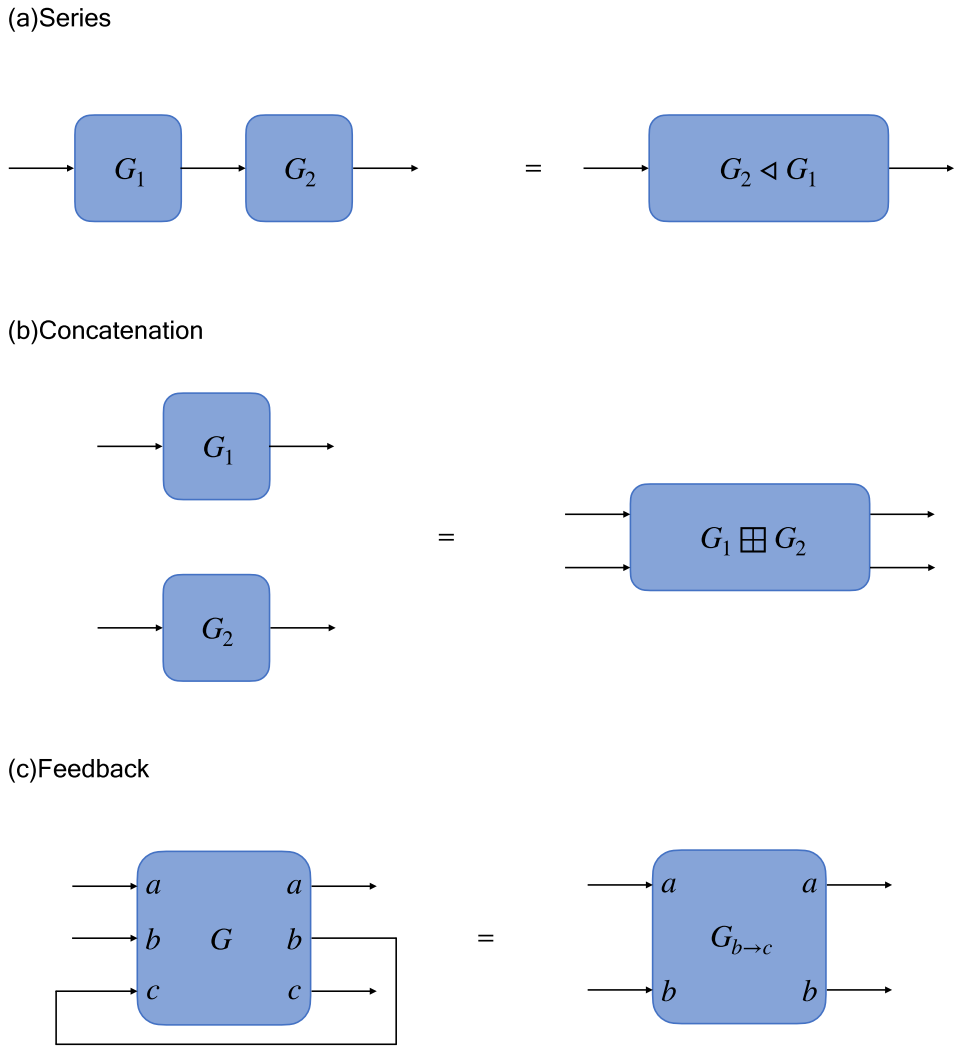

Figure 2.1: Three operations in SLH rules: (a) series $G_2 \triangleleft G_1$; (b) concatenation $G_1 \boxplus G_2$; (c) feedback $G_b \to G_c$.

have independent input and output fields. The resulting system is

$$G_1 \boxplus G_2 = \left(\begin{bmatrix} \mathbf{S}_1 & 0 \\ 0 & \mathbf{S}_2 \end{bmatrix}, \begin{bmatrix} \mathbf{L}_1 \\ \mathbf{L}_2 \end{bmatrix}, H_1 + H_2 \right). \tag{2.25}$$

A generalization of the concatenation product is direct coupling, where there is an interaction H_{int} between the two components. Here, H_1 is replaced by $H_1 + H_{\text{int}}$.

The most complicated interconnection is feedback, which describes that the b-th output of a component is the c-th input of the same component. This interconnection is denoted by $b \to c$. The triplet of the result $\tilde{G} = (\tilde{\mathbf{S}}, \tilde{\mathbf{L}}, \tilde{H})$ with this eliminated interconnection is

$$\tilde{\mathbf{S}} = \mathbf{S}_{\not b,\not c} + \mathbf{S}_{\not b,c}(I - S_{b,c})^{-1}\mathbf{S}_{b,\not c}, \tag{2.26}$$

$$\tilde{\mathbf{L}} = \mathbf{L}_{\not b} + \mathbf{S}_{\not b,c}(I - S_{b,c})^{-1}L_b, \tag{2.27}$$

$$\tilde{H} = H + \frac{1}{2i}(\mathbf{L}^\dagger \mathbf{S}_{:,c}(I - S_{b,c})^{-1} L_b - L_b^\dagger (I - S_{b,c}^\dagger)^{-1} \mathbf{S}_{:,c}^\dagger \mathbf{L}), \tag{2.28}$$

where $S_{b,c}$ is the bc element; $\mathbf{S}_{:,c}$ is the cth column; $\mathbf{S}_{b',c'}$ is the scattering matrix without the bth row and cth column; $\mathbf{S}_{b',c}$ and $\mathbf{S}_{b,c'}$ are the cth column with the bth row deleted and the bth row with the c column deleted, of $\mathbf{S}$, respectively; $\mathbf{L}_{b'}$ is $\mathbf{L}$ without the bth row; L_b is the bth row of $\mathbf{L}$. Here, b, c indicate sets, when the component has multiple eliminated ports.

Finally, with these three rules, some quantum networks can be described. This kind of quantum networks should satisfy three conditions: the Born-Markov approximation; the propagation time between components can be neglected compared to the relaxation times of the systems; and the propagation fields are bosonic in a linear medium without dispersion. Finally, we can extract the master equation from the triplet $G = (\mathbf{S}, \mathbf{L}, H)$ of the network in the form

$$\frac{\mathrm{d}}{\mathrm{d}t}\rho = -i[H, \rho] + \sum_{k=1} \mathcal{D}[L_k]\rho, . \tag{2.29}$$

The definition of $\mathcal{D}[L_k]\rho$ is shown in Sec. 2.1.1, therefore, the relaxation rate can be obtained.

2.3 Atoms in an ideal continuous waveguide

We now present the application of the SLH formalism to both small and giant atoms coupled to an ideal continuous waveguide. Our analysis begin with a single giant atom featuring two coupling points, subsequently moving to two-atom systems.

2.3.1 A single giant atom

First, we consider a single giant atom A with resonant frequency ω_a. In this thesis, the atoms are two-level systems, so the Hamiltonian of the atom is

$$H_a = \frac{\omega_a}{2}\sigma_z^a. \tag{2.30}$$

The relaxation rate of the atom associated with the coupling point n is denoted by γ_n, referred to as the bare relaxation rate. Since there are left- and right-propagating modes in the waveguide, the relaxation through this coupling point can be divided into the rates γ_{nR} and γ_{nL}, which satisfy $\gamma_{nR} + \gamma_{nL} = \gamma_n$. The phase shift between neighboring coupling points is denoted by $\phi_n = kd_n$ for $n = 1, 2 \ldots$, where k is the wave number and d_n is the distance between neighboring coupling points n and $n + 1$.

We define an SLH triplet at each coupling point:

$$G_{nR/L} = \begin{cases} \left(1, \sqrt{\gamma_{nR/L}}\sigma_-^j, \frac{1}{2}\omega_j \sigma_z^j\right) & \text{if } n \text{ is the first coupling point of} \\ & \text{atom } j \text{ from the right side} \\ \left(1, \sqrt{\gamma_{nR/L}}\sigma_-^j, 0\right) & \text{otherwise.} \end{cases} \tag{2.31}$$

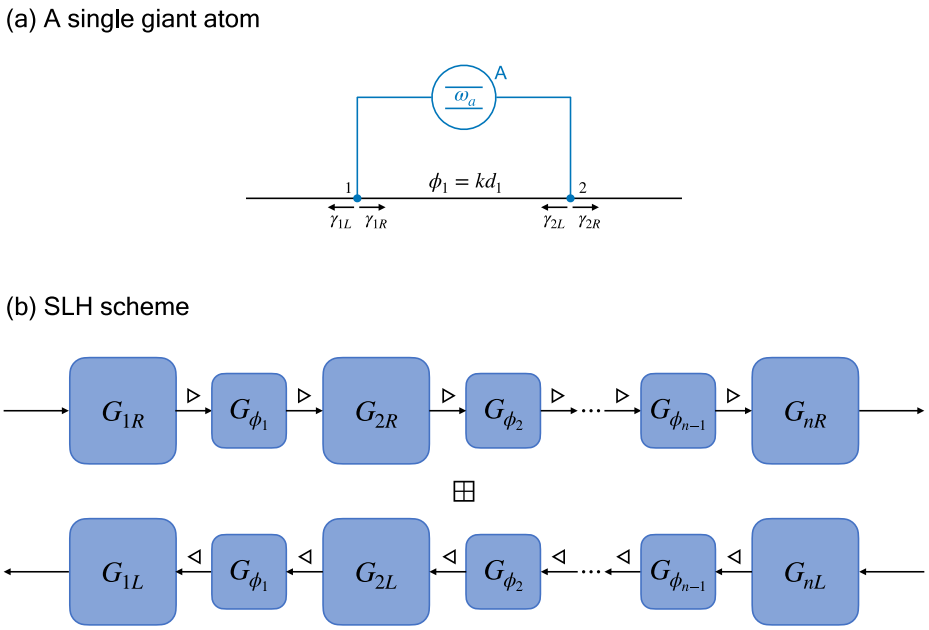

Figure 2.2: (a) A single giant atom coupled to an ideal waveguide. (b) A general SLH scheme for an arbitrary number of giant atoms couple to an ideal waveguide with an arbitrary number of coupling points. For the specific case of a single giant atom with two coupling points analyzed in this section, $n = 2$. Figures adapted from Ref. [6].

The phase shift is defined as $G_{\phi_n} = (e^{i\phi_n}, 0, 0)$. As this is a cascaded system, a series product is performed between all components, and accounting for two anti-parallel traveling modes (right and left) in the system, we apply a concatenation product between these two modes. For simplicity, in this section we only discuss a single giant atom with two coupling points. Then, the SLH triplet of Fig. 2.2a can be obtained from the following components:

$$\begin{aligned} G_R &= G_{2R} \lhd G_{\phi_1} \lhd G_{1R} \\ &= \left(1, \sqrt{\gamma_{2R}}\sigma_-^a, 0\right) \lhd \left(e^{i\phi_1}, 0, 0\right) \lhd \left(1, \sqrt{\gamma_{1R}}\sigma_-^a, \tfrac{1}{2}\omega_a\sigma_z^a\right), \end{aligned} \tag{2.32}$$

$$\begin{aligned} G_L &= G_{1L} \lhd G_{\phi_1} \lhd G_{2L} \\ &= \left(1, \sqrt{\gamma_{1L}}\sigma_-^a, 0\right) \lhd \left(e^{i\phi_1}, 0, 0\right) \lhd \left(1, \sqrt{\gamma_{2L}}\sigma_-^a, 0\right), \end{aligned} \tag{2.33}$$

the result $G_a = G_R \boxplus G_L$ is

$$\begin{aligned} \mathbf{S}_a &= \begin{pmatrix} e^{i\phi_1} & 0 \\ 0 & e^{i\phi_1} \end{pmatrix}, \\ \mathbf{L}_a &= \begin{pmatrix} \left(e^{i\phi_1}\sqrt{\gamma_{1R}} + \sqrt{\gamma_{2R}}\right)\sigma_-^a \\ \left(\sqrt{\gamma_{1L}} + e^{i\phi_1}\sqrt{\gamma_{2L}}\right)\sigma_-^a \end{pmatrix}, \\ H_a &= \frac{1}{2}\omega_a\sigma_z^a + \frac{1}{2}(\sqrt{\gamma_{1R}\gamma_{2R}} + \sqrt{\gamma_{1L}\gamma_{2L}})\sin\phi_1\sigma_z^a. \end{aligned} \tag{2.34}$$

So the master equation extracted from Eq. (2.34) is

$$\begin{aligned}\dot{\rho} &= -i\left[H_a, \rho\right] + \mathcal{D}\left[\left(e^{i\phi_1}\sqrt{\gamma_{1R}} + \sqrt{\gamma_{2R}}\right)\sigma_-^a\right]\rho + \mathcal{D}\left[\left(\sqrt{\gamma_{1L}} + e^{i\phi_1}\sqrt{\gamma_{2L}}\right)\sigma_-^a\right]\rho \\ &= -i\left[\frac{\omega_a + \left(\sqrt{\gamma_{1R}\gamma_{2R}} + \sqrt{\gamma_{1L}\gamma_{2L}}\right)\sin\phi_1}{2}\sigma_z^a, \rho\right] + \Gamma_a\mathcal{D}\left[\sigma_-^a\right]\rho,\end{aligned} \tag{2.35}$$

where the atom Hamiltonian is introduced to a Lamb shift determined by the bare relaxation rates and phase shift, and the effective relaxation rate is

$$\Gamma_a = \left|\sqrt{\gamma_{1R}} + e^{i\phi_1}\sqrt{\gamma_{2R}}\right|^2 + \left|\sqrt{\gamma_{1L}} + e^{i\phi_1}\sqrt{\gamma_{2L}}\right|^2. \tag{2.36}$$

Sec. 2.3.3.1 provides a comprehensive analysis of the relaxation rates.

2.3.2 Two atoms

In this section, we introduce two atoms coupled to the waveguide, including both small and giant atoms (shown in Fig. 2.3). For two giant atoms with two coupling points each, we investigate three possible arrangements of atoms: the separate configuration (Fig. 2.3b), where the second atom's coupling points follow those of the first atom sequentially;the nested configuration (Fig. 2.3d), where the second atom's points are enclosed by the first atom's; the braided configuration (Fig. 2.3c) that we previously mentioned in Sec. 1.1.

Here, we only detail the calculation of the braided configuration. Moreover, the results of the separate and nested configuration are shown in Table 2.1. We set

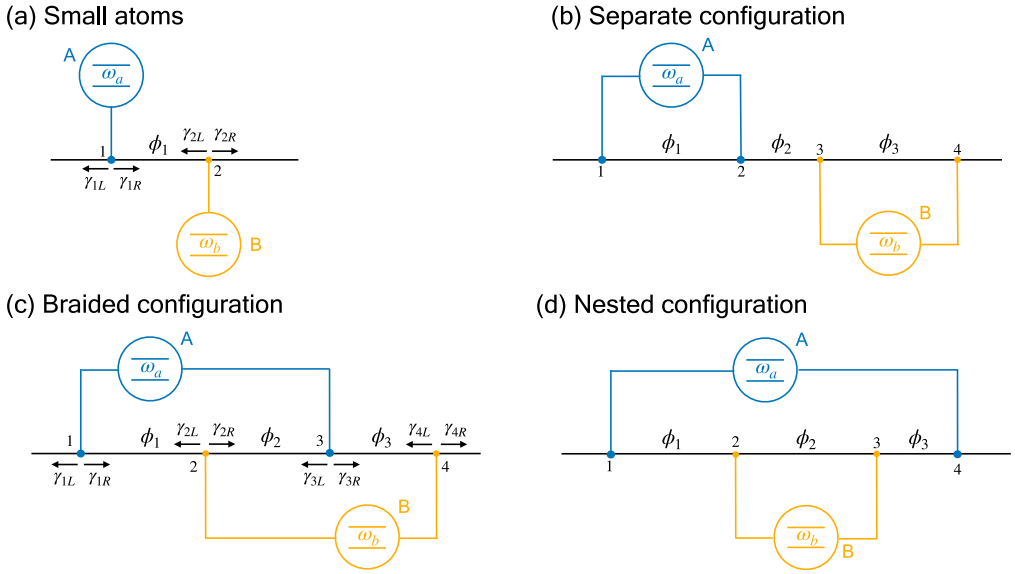

Figure 2.3: Different topologies of two atoms couple to an ideal waveguide. (a) Sketch of two small atoms; (b-d) sketches of braided, separate, nested atoms. Figures adapted from Ref. [6].

two atoms A and B with resonant frequencies ω_a and ω_b, respectively. Then the

Hamiltonian is

$$H_j = \frac{\omega_j}{2}\sigma_z^j, \tag{2.37}$$

where j represents the index of the atom.

Similar to the case of a single giant atom, we obtain

$$\begin{aligned} G_R\big|_{\text{small}} &= G_{2R} \lhd G_{\phi_1} \lhd G_{1R} \\ &= \left(1, \sqrt{\gamma_{2R}}\sigma_-^b, \frac{1}{2}\omega_b\sigma_z^b\right) \lhd \left(e^{i\phi_1}, 0, 0\right) \lhd \left(1, \sqrt{\gamma_{1R}}\sigma_-^a, \frac{1}{2}\omega_a\sigma_z^a\right), \end{aligned} \tag{2.38}$$

$$\begin{aligned} G_L\big|_{\text{small}} &= G_{1L} \lhd G_{\phi_1} \lhd G_{2L} \\ &= \left(1, \sqrt{\gamma_{1L}}\sigma_-^a, 0\right) \lhd \left(e^{i\phi_1}, 0, 0\right) \lhd \left(1, \sqrt{\gamma_{2L}}\sigma_-^b, 0\right). \end{aligned} \tag{2.39}$$

For giant atoms in the braided configuration, we have

$$\begin{aligned} G_R\big|_{\text{braided}} &= G_{4R} \lhd G_{\phi_3} \lhd G_{3R} \lhd G_{\phi_2} \lhd G_{2R} \lhd G_{\phi_1} \lhd G_{1R} \\ &= \left(1, \sqrt{\gamma_{4R}}\sigma_-^b, 0\right) \lhd \left(e^{i\phi_3}, 0, 0\right) \lhd \left(1, \sqrt{\gamma_{3R}}\sigma_-^a, 0\right) \lhd \left(e^{i\phi_2}, 0, 0\right) \\ &\quad \lhd \left(1, \sqrt{\gamma_{2R}}\sigma_-^b, \frac{1}{2}\omega_b\sigma_z^b\right) \lhd \left(e^{i\phi_1}, 0, 0\right) \lhd \left(1, \sqrt{\gamma_{1R}}\sigma_-^a, \frac{1}{2}\omega_a\sigma_z^a\right), \end{aligned} \tag{2.40}$$

$$\begin{aligned} G_L\big|_{\text{braided}} &= G_{1L} \lhd G_{\phi_1} \lhd G_{2L} \lhd G_{\phi_2} \lhd G_{3L} \lhd G_{\phi_3} \lhd G_{4L} \\ &= \left(1, \sqrt{\gamma_{1L}}\sigma_-^a, 0\right) \lhd \left(e^{i\phi_1}, 0, 0\right) \lhd \left(1, \sqrt{\gamma_{2L}}\sigma_-^b, 0\right) \lhd \left(e^{i\phi_2}, 0, 0\right) \\ &\quad \lhd \left(1, \sqrt{\gamma_{3L}}\sigma_-^a, 0\right) \lhd \left(e^{i\phi_3}, 0, 0\right) \lhd \left(1, \sqrt{\gamma_{1L}}\sigma_-^b, 0\right). \end{aligned} \tag{2.41}$$

The results for small and braided atoms are shown below, respectively,

$$\begin{aligned} \mathbf{S}\big|_{\text{small}} &= \begin{pmatrix} e^{i\phi_1} & 0 \\ 0 & e^{i\phi_1} \end{pmatrix}, \\ \mathbf{L}\big|_{\text{small}} &= \begin{pmatrix} e^{i\phi_1}\sqrt{\gamma_{1R}}\sigma_-^a + \sqrt{\gamma_{2R}}\sigma_-^b \\ \sqrt{\gamma_{1L}}\sigma_-^a + e^{i\phi_1}\sqrt{\gamma_{2L}}\sigma_-^b \end{pmatrix}, \\ H\big|_{\text{small}} &= \frac{1}{2}\omega_a\sigma_z^a + \frac{1}{2}\omega_b\sigma_z^b + \frac{1}{2i}\left[\left(e^{i\phi_1}\sqrt{\gamma_{1R}\gamma_{2R}} - e^{-i\phi_1}\sqrt{\gamma_{1L}\gamma_{2L}}\right)\sigma_-^a\sigma_+^b - \text{H.c.}\right], \end{aligned} \tag{2.42}$$

$$
\begin{aligned}
\mathbf{S}\big|_{\text{braided}} &= \begin{pmatrix} e^{i(\phi_1+\phi_2+\phi_3)} & 0 \\ 0 & e^{i(\phi_1+\phi_2+\phi_3)} \end{pmatrix}, \\
\mathbf{L}\big|_{\text{braided}} &= \begin{pmatrix} \left(e^{i(\phi_1+\phi_2+\phi_3)}\sqrt{\gamma_{1R}} + e^{i\phi_3}\sqrt{\gamma_{3R}}\right)\sigma_-^a + \left(e^{i(\phi_2+\phi_3)}\sqrt{\gamma_{2R}} + \sqrt{\gamma_{4R}}\right)\sigma_-^b \\ \left(\sqrt{\gamma_{1L}} + e^{i(\phi_1+\phi_2)}\sqrt{\gamma_{3L}}\right)\sigma_-^a + \left(e^{i\phi_1}\sqrt{\gamma_{2L}} + e^{i(\phi_1+\phi_2+\phi_3)}\sqrt{\gamma_{4L}}\right)\sigma_-^b \end{pmatrix}, \\
H\big|_{\text{braided}} &= \frac{1}{2}\left(\omega_a + \left(\sqrt{\gamma_{1R}\gamma_{3R}} + \sqrt{\gamma_{1L}\gamma_{3L}}\right)\sin\left(\phi_1+\phi_2\right)\right)\sigma_z^a \\
&\quad + \frac{1}{2}\left(\omega_b + \left(\sqrt{\gamma_{2R}\gamma_{4R}} + \sqrt{\gamma_{2L}\gamma_{4L}}\right)\sin\left(\phi_2+\phi_3\right)\right)\sigma_z^b \\
&\quad + \frac{1}{2i}\Big[\Big(e^{i\phi_1}\sqrt{\gamma_{1R}\gamma_{2R}} + e^{i(\phi_1+\phi_2+\phi_3)}\sqrt{\gamma_{1R}\gamma_{4R}} - e^{-i\phi_2}\sqrt{\gamma_{2R}\gamma_{3R}} \\
&\qquad + e^{i\phi_3}\sqrt{\gamma_{3R}\gamma_{4R}} - e^{-i\phi_1}\sqrt{\gamma_{1L}\gamma_{2L}} - e^{-i(\phi_1+\phi_2+\phi_3)}\sqrt{\gamma_{1L}\gamma_{4L}} \\
&\qquad + e^{i\phi_2}\sqrt{\gamma_{2L}\gamma_{3L}} - e^{-i\phi_3}\sqrt{\gamma_{3L}\gamma_{4L}}\Big)\sigma_-^a\sigma_+^b - \text{H.c.}\Big].
\end{aligned}
\tag{2.43}
$$

Finally, from the triplet components above, we can extract the master equation in the following form

$$
\begin{aligned}
\dot{\rho} &= -i\left[H,\rho\right] + \sum_j \mathcal{D}[L_j]\rho \\
&= -i\left[\frac{1}{2}\omega_a'\sigma_z^a + \frac{1}{2}\omega_b'\sigma_z^b + g\sigma_-^a\sigma_+^b + g^*\sigma_+^a\sigma_-^b\right] \\
&\quad + \Gamma_a\mathcal{D}[\sigma_-^a]\rho + \Gamma_b\mathcal{D}[\sigma_-^b]\rho + \left[\Gamma_{\text{coll}}\left(\sigma_-^a\rho\sigma_+^b - \frac{1}{2}\left\{\sigma_-^a\sigma_+^b,\rho\right\}\right) + \text{H.c.}\right],
\end{aligned}
\tag{2.44}
$$

where, ω_j' is the Lamb-shifted frequency of the atom j, Γ_j is its individual relaxation rate, Γ_{coll} is the collective relaxation rate for the atoms, and g is the exchange interaction between two different atoms, which arises when the emitted photons of one atom are absorbed at the coupling points of the other atom. According to Eq. (2.44), the individual relaxation rates Γ_a, Γ_b are determined by interference between coupling points belonging to the same atom, while the collective relaxation rate Γ_{coll} is determined by interference between coupling points from different atoms. Note that the former case occurs only for giant atoms. The expressions of these parameters for other topologies are shown in Table 2.1.

Table 2.1: General expressions of frequency shifts, individual and collective relaxation rates and exchange interactions for different topologies. Here, two small and giant atoms couple to an ideal waveguide. We set phase shifts ϕ_n acquired in the waveguide and bare relaxation rates γ_{nR} and γ_{nL} at each coupling point. Adapted from Ref. [6].

Parameters	Topologies	Expressions
Frequency shifts (δ_{ω_a}, δ_{ω_b})	Small	0 0

Continued on next page

Table 2.1 – continued from previous page

Parameters	Topologies	Expressions
	Separate	$(\sqrt{\gamma_{1R}\gamma_{2R}} + \sqrt{\gamma_{1L}\gamma_{2L}}) \sin\phi_1$
		$(\sqrt{\gamma_{3R}\gamma_{4R}} + \sqrt{\gamma_{3L}\gamma_{4L}}) \sin\phi_3$
	Braided	$(\sqrt{\gamma_{1R}\gamma_{3R}} + \sqrt{\gamma_{1L}\gamma_{3L}}) \sin(\phi_1+\phi_2)$
		$(\sqrt{\gamma_{2R}\gamma_{4R}} + \sqrt{\gamma_{2L}\gamma_{4L}}) \sin(\phi_2+\phi_3)$
	Nested	$(\sqrt{\gamma_{1R}\gamma_{4R}} + \sqrt{\gamma_{1L}\gamma_{4L}}) \sin(\phi_1+\phi_2+\phi_3)$
		$(\sqrt{\gamma_{2R}\gamma_{3R}} + \sqrt{\gamma_{2L}\gamma_{3L}}) \sin\phi_2$
Individual relaxation rates (Γ_a, Γ_b)	Small	$\gamma_{1R} + \gamma_{1L}$
		$\gamma_{2R} + \gamma_{2L}$
	Separate	$\gamma_{1R} + \gamma_{2R} + \gamma_{1L} + \gamma_{2L}$
		$+2(\sqrt{\gamma_{1R}\gamma_{2R}} + \sqrt{\gamma_{1L}\gamma_{2L}}) \cos\phi_1$
		$\gamma_{3R} + \gamma_{4R} + \gamma_{3L} + \gamma_{4L}$
		$+2(\sqrt{\gamma_{3R}\gamma_{4R}} + \sqrt{\gamma_{3L}\gamma_{4L}}) \cos\phi_3$
	Braided	$\gamma_{1R} + \gamma_{3R} + \gamma_{1L} + \gamma_{3L}$
		$+2(\sqrt{\gamma_{1R}\gamma_{3R}} + \sqrt{\gamma_{1L}\gamma_{3L}}) \cos(\phi_1+\phi_2)$
		$\gamma_{2R} + \gamma_{4R} + \gamma_{2L} + \gamma_{4L}$
		$+2(\sqrt{\gamma_{2R}\gamma_{4R}} + \sqrt{\gamma_{2L}\gamma_{4L}}) \cos(\phi_2+\phi_3)$
	Nested	$\gamma_{1R} + \gamma_{4R} + \gamma_{1L} + \gamma_{4L}$
		$+2(\sqrt{\gamma_{1R}\gamma_{4R}} + \sqrt{\gamma_{1L}\gamma_{4L}}) \cos(\phi_1+\phi_2+\phi_3)$
		$\gamma_{2R} + \gamma_{3R} + \gamma_{2L} + \gamma_{3L}$
		$+2(\sqrt{\gamma_{2R}\gamma_{4R}} + \sqrt{\gamma_{2L}\gamma_{4L}}) \cos\phi_2$
Collective relaxation rates (Γ_{coll})	Small	$e^{i\phi_1}\sqrt{\gamma_{1R}\gamma_{2R}} + e^{-i\phi_1}\sqrt{\gamma_{1L}\gamma_{2L}}$
	Separate	$e^{i(\phi_1+\phi_2)}\sqrt{\gamma_{1R}\gamma_{3R}} + e^{i(\phi_2+\phi_3)}\sqrt{\gamma_{2R}\gamma_{4R}}$
		$+e^{i(\phi_1+\phi_2+\phi_3)}\sqrt{\gamma_{1R}\gamma_{4R}} + e^{i\phi_2}\sqrt{\gamma_{2R}\gamma_{3R}}$
		$+e^{-i(\phi_1+\phi_2)}\sqrt{\gamma_{1L}\gamma_{3L}} + e^{-i(\phi_2+\phi_3)}\sqrt{\gamma_{2L}\gamma_{4L}}$
		$+e^{-i(\phi_1+\phi_2+\phi_3)}\sqrt{\gamma_{1L}\gamma_{4L}} + e^{-i\phi_2}\sqrt{\gamma_{2L}\gamma_{3L}}$
	Braided	$e^{i\phi_1}\sqrt{\gamma_{1R}\gamma_{2R}} + e^{i(\phi_1+\phi_2+\phi_3)}\sqrt{\gamma_{1R}\gamma_{4R}}$
		$+e^{-i\phi_2}\sqrt{\gamma_{2R}\gamma_{3R}} + e^{i\phi_3}\sqrt{\gamma_{3R}\gamma_{4R}}$
		$+e^{-i\phi_1}\sqrt{\gamma_{1L}\gamma_{2L}} + e^{-i(\phi_1+\phi_2+\phi_3)}\sqrt{\gamma_{1L}\gamma_{4L}}$
		$+e^{i\phi_2}\sqrt{\gamma_{2L}\gamma_{3L}} + e^{-i\phi_3}\sqrt{\gamma_{3L}\gamma_{4L}}$

Continued on next page

Table 2.1 – continued from previous page

Parameters	Topologies	Expressions
	Nested	$e^{i\phi_1}\sqrt{\gamma_{1R}\gamma_{2R}} + e^{i(\phi_1+\phi_2)}\sqrt{\gamma_{1R}\gamma_{3R}}$ $+e^{-i(\phi_2+\phi_3)}\sqrt{\gamma_{2R}\gamma_{4R}} + e^{-i\phi_3}\sqrt{\gamma_{3R}\gamma_{4R}}$ $+e^{-i\phi_1}\sqrt{\gamma_{1L}\gamma_{2L}} + e^{-i(\phi_1+\phi_2)}\sqrt{\gamma_{1L}\gamma_{3L}}$ $+e^{i(\phi_2+\phi_3)}\sqrt{\gamma_{2L}\gamma_{4L}} + e^{i\phi_3}\sqrt{\gamma_{3L}\gamma_{4L}}$
Exchange interactions (g)	Small	$(e^{i\phi_1}\sqrt{\gamma_{1R}\gamma_{2R}} - e^{-i\phi_1}\sqrt{\gamma_{1L}\gamma_{2L}})/(2i)$
	Separate	$(e^{i(\phi_1+\phi_2)}\sqrt{\gamma_{1R}\gamma_{3R}} + e^{i(\phi_1+\phi_2+\phi_3)}\sqrt{\gamma_{1R}\gamma_{4R}}$ $+e^{i\phi_2}\sqrt{\gamma_{2R}\gamma_{3R}} + e^{i(\phi_2+\phi_3)}\sqrt{\gamma_{2R}\gamma_{4R}}$ $-e^{-i(\phi_1+\phi_2)}\sqrt{\gamma_{1L}\gamma_{3L}} - e^{-i(\phi_1+\phi_2+\phi_3)}\sqrt{\gamma_{1L}\gamma_{4L}}$ $-e^{-i\phi_2}\sqrt{\gamma_{2L}\gamma_{3L}} - e^{-i(\phi_2+\phi_3)}\sqrt{\gamma_{2L}\gamma_{4L}})/(2i)$
	Braided	$(e^{i\phi_1}\sqrt{\gamma_{1R}\gamma_{2R}} + e^{i(\phi_1+\phi_2+\phi_3)}\sqrt{\gamma_{1R}\gamma_{4R}}$ $-e^{-i\phi_2}\sqrt{\gamma_{2R}\gamma_{3R}} + e^{i\phi_3}\sqrt{\gamma_{3R}\gamma_{4R}}$ $-e^{-i\phi_1}\sqrt{\gamma_{1L}\gamma_{2L}} - e^{-i(\phi_1+\phi_2+\phi_3)}\sqrt{\gamma_{1L}\gamma_{4L}}$ $+e^{i\phi_2}\sqrt{\gamma_{2L}\gamma_{3L}} - e^{-i\phi_3}\sqrt{\gamma_{3L}\gamma_{4L}})/(2i)$
	Nested	$(e^{i\phi_1}\sqrt{\gamma_{1R}\gamma_{2R}} + e^{i(\phi_1+\phi_2)}\sqrt{\gamma_{1R}\gamma_{3R}}$ $-e^{-i(\phi_2+\phi_3)}\sqrt{\gamma_{2R}\gamma_{4R}} - e^{-i\phi_3}\sqrt{\gamma_{3R}\gamma_{4R}}$ $-e^{-i\phi_1}\sqrt{\gamma_{1L}\gamma_{2L}} - e^{-i(\phi_1+\phi_2)}\sqrt{\gamma_{1L}\gamma_{3L}}$ $+e^{i(\phi_2+\phi_3)}\sqrt{\gamma_{2L}\gamma_{4L}} + e^{i\phi_3}\sqrt{\gamma_{3L}\gamma_{4L}})/(2i)$

2.3.3 Decoherence-free interaction and dark states

When the relaxation rates are non-zero, the atoms have interactions with the waveguide and lose energy to it. Here, we look into two approaches for protecting the system against decoherence: decoherence-free interaction and dark states. Note that in realistic experiments, decoherence has two mechanisms: energy relaxation and phase dephasing [30]. In this thesis, however, we consider the relaxation as the only loss channel, then when we talk about suppressing decoherence, it is equivalent to suppressing relaxation.

2.3.3.1 Decoherence-free interaction

According to Eq. (2.36) and Table 2.1, the individual and collective relaxation rates can be controlled by tuning the phase shift ϕ_n between the coupling points. If we assume all the bare relaxation rates are equal, i.e., $\gamma_{nR} = \gamma_{nL} = \gamma$, for giant atoms, the individual relaxation rates Γ_j can be suppressed to 0 by setting the phase shift between the coupling points of the same atom to $\pi(+2n\pi)$, corresponding to a spatial

separation of half the excitation wavelength, $\lambda/2(+\lambda)$. Since relaxation is considered the only decoherence mechanism, we characterize the atom as *decoherence-free*.

For an atomic ensemble, emissions from different coupling points of the same atom undergo destructive interference, resulting in a vanishing contribution from all atoms and thereby protecting the system from collective relaxation. Furthermore, in both separate and nested configurations, at least one atom has consecutive coupling points. When the emission from this atom is canceled ($\Gamma_j = 0$), the exchange interaction also vanishes, i.e., $g = 0$. In contrast, braided giant atoms can exhibit interactions without decoherence, characterized by $\Gamma_j = \Gamma_{\text{coll}} = 0$ while $g \neq 0$. Fig. 2.4 intuitively shows this phenomenon: decoherence-free interaction (DFI).

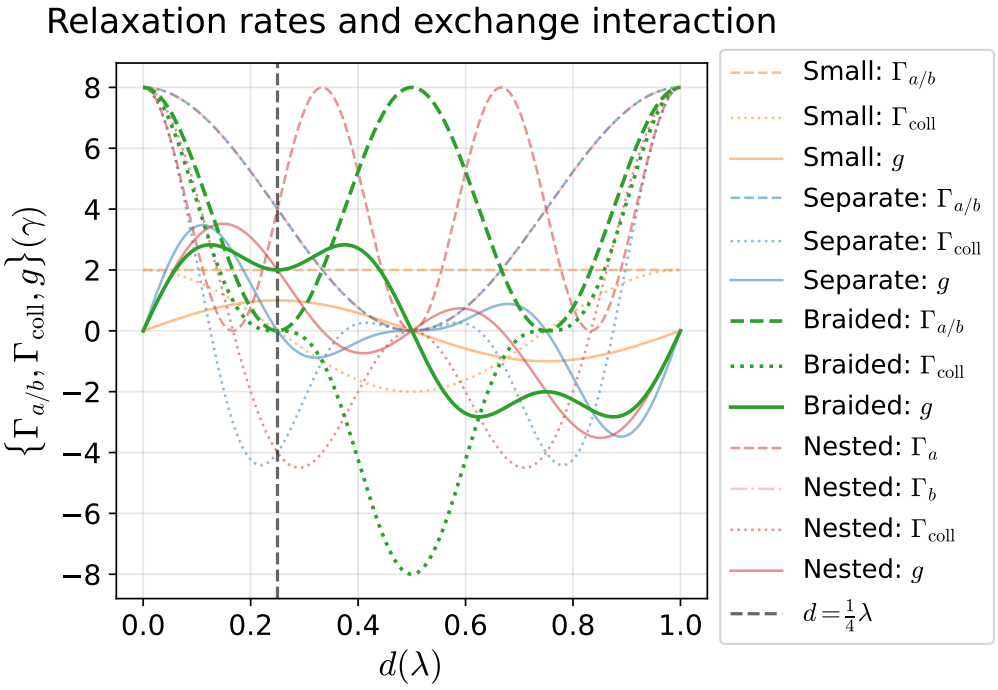

Figure 2.4: Illustration of relaxation rates and exchange interaction for two atoms coupled to an ideal waveguide across all topologies. The dashed dark line indicates $d = \lambda/4$ where decoherence-free interaction occurs. The transparent orange, blue and red lines correspond to small, separate and nested atom configurations, respectively, while the green lines represent braided atoms. Figure inspired by Ref. [8].

Note that, according to the supplemental material of Ref. [8] and Ref. [6], these conclusions also remain valid for arbitrary bare relaxation rates, provided that the condition $\Gamma_j = 0$ is satisfied. Because the decoherence-free interaction does not depend on the quantum state of the giant atoms, the entire Hilbert space of the system is protected from decoherence.

2.3.3.2 Dark states

Besides the DFI, a less robust mechanism for protecting the system from decoherence is dark states, which arise from collective interference [12] and depend on the state

of the atoms. Note first that dark states can be realized both with small atoms and giant atoms. As a result, only a Hilbert subspace is protected from decoherence. Pure non-radiative dark states $|D\rangle$ are annihilated by all jump operators and, at the same time, are eigenstates of the Hamiltonian, [12, 15, 16, 31, 32], i.e.,

$$L_{R/L}\,|D\rangle = 0, \tag{2.45}$$

$$H\,|D\rangle = E\,|D\rangle\,, E \in \mathbb{R}. \tag{2.46}$$

The first condition ensures that system's output remains dark, while the second guarantees that the system is stationary. In the two-atom case considered here, Eq. (2.45) implies that the dark states reside within a two-dimensional subspace. This subspace is spanned by the ground state $|gg\rangle$ and either the singlet state $|S\rangle = (|ge\rangle - |eg\rangle)/\sqrt{2}$ or the triplet state $|T\rangle = (|ge\rangle + |eg\rangle)/\sqrt{2}$.

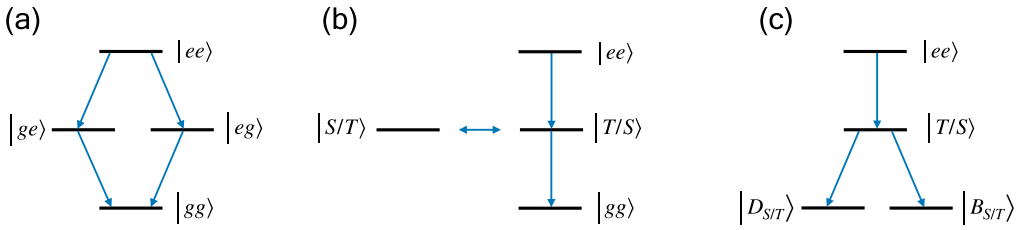

Figure 2.5: Energy-level diagrams of two two-level atoms coupled to a waveguide. (a) This figure shows the a basis of states is $\{|gg\rangle\,, |eg\rangle\,, |ge\rangle\,, |ee\rangle\}$, including their decay channels. (b) Diagram for a undriven system, the dark states $|S/T\rangle$ do not decay to the waveguide, while $|T/S\rangle$ act as bright states. (c) Diagram for the driven-dissipative regime, and the dark states $\left|D_{S/T}\right\rangle$ is defined by Eq. (2.53). Figures adapted from Ref. [6].

Undriven system

In an undriven system, the dark state is either the singlet state $|S\rangle$ or the triplet state $|T\rangle$, depending on the phase shifts acquired by the distances between the coupling points. To derive the corresponding constraints, we rewrite the Hamiltonian and jump operators in the basis $\{|gg\rangle\,, |S\rangle\,, |T\rangle\,, |ee\rangle\}$ (Fig. 2.5b). The Hamiltonian then takes the form

$$\begin{aligned} H = H_u &= \frac{1}{2}\omega_a'\sigma_z^a + \frac{1}{2}\omega_b'\sigma_z^b + g\sigma_-^a\sigma_+^b + g^*\sigma_+^a\sigma_-^b \\ &= \frac{\omega_a' + \omega_b'}{2}(|ee\rangle\langle ee| - |gg\rangle\langle gg|) \\ &\quad + \frac{g + g^*}{2}(|T\rangle\langle T| - |S\rangle\langle S|) \\ &\quad + \left[\frac{\omega_b' - \omega_a' + g - g^*}{2}\,|S\rangle\langle T| + \text{H.c.}\right]. \end{aligned} \tag{2.47}$$

In the same way, the jump operators can be written as

$$\begin{aligned} L_{R/L} &= \sqrt{\Gamma_{aR/L}}\sigma_-^a + \sqrt{\Gamma_{aR/L}}\sigma_-^b \\ &= \frac{\sqrt{2}}{2}(\sqrt{\Gamma_{aR/L}} + \sqrt{\Gamma_{bR/L}})(|T\rangle\langle ee| - |gg\rangle\langle T|) \\ &\quad + \frac{\sqrt{2}}{2}(\sqrt{\Gamma_{aR/L}} - \sqrt{\Gamma_{bR/L}})(|S\rangle\langle ee| - |gg\rangle\langle S|). \end{aligned} \tag{2.48}$$

Substituting these expressions for jump operators and the Hamiltonian into the dark-state conditions, Eq. (2.45) and Eq. (2.46), yields the constraints on $\gamma_{kR/L}$, ϕ_k and ω_j. The remaining steps are mathematical derivations, and Ref. [6] shows the details. For simplicity, we assume that the bare relaxation rates are identical for all coupling points in the same propagation direction, i.e., $\gamma_{nR} = \gamma_R$, $\gamma_{nL} = \gamma_L$. According to the calculation, all topologies require $\omega_a = \omega_b$, $g = g^* \in \mathbb{R}$, while the additional constraints are summarized in Table B.1 in Appendix B.

As shown in Table B.2, constraints on bare relaxation rates are required to achieve symmetric couplings. Because of the perfectly symmetric distribution of coupling points, the nested atoms allow the formation of dark states for arbitrary bare relaxation rates, offering increased flexibility for implementation.

Coherently driven system

Refs. [12, 15, 16] have investigated the formation of dark states for small atoms in the driven-dissipative regime. Ref. [6] further showed that such states can also be realized in giant-atom systems. When a coherent drive is applied from the left side of the waveguide, the system eventually reaches a dynamic equilibrium between coherent driving and dissipation, formed by mutually exchanging photons between the atoms [14]. For convenience in getting the constraints of dark states in the driven-dissipative regime, we still rewrite Hamiltonians and operators in the basis shown in Fig. 2.5b.

The drive is characterized by a bosonic flux of $|\beta|^2$ photons per second and is described by the triplet $G_\beta = (\beta, 0, 0)$. Within the SLH formalism, the additional term of Hamiltonian is

$$H_{\text{drive}} = -\frac{i}{2}\beta S_R L_R^\dagger + \text{H.c.}, \tag{2.49}$$

while the corresponding jump operator is

$$\mathbf{L} = \begin{pmatrix} L_R + L_d \\ L_L \end{pmatrix}, \tag{2.50}$$

where $L_d = \beta S_R$. Expanding the Lindblad master equation with L_d and H_{drive}, the dynamics of this system are the same as the system with the master equation

$$\dot{\rho} = -i[H_u + H_d, \rho] + \mathcal{D}[L_R]\rho + \mathcal{D}[L_L]\rho, \tag{2.51}$$

where H_d is

$$H_d = -i\beta S_R L_R^\dagger + \text{H.c.}. \tag{2.52}$$

For convenience, we can use the latter to derive the dark states, with the details provided in Appendix A. Then the total Hamiltonian is $H = H_d + H_u$, where H_u is the Hamiltonian without drive. In the presence of a coherent drive, the dark states satisfy the same conditions as those given in Eq. (2.45) and Eq. (2.46), and take the form

$$\left|D_{S/T}\right\rangle = \frac{1}{\sqrt{1+\alpha^2}}\left(\alpha\left|S/T\right\rangle + \left|gg\right\rangle\right), \tag{2.53}$$

where α depends on the bare relaxation rates, detuning of the atomic frequencies from the drive, and the drive strength. We denote the detuning of the atomic frequency from the drive by δ_j, such that $\omega_j = \omega_d + \delta_j$. Moreover, the state $\left|D_{S/T}\right\rangle$ only exists when the two detunings are opposite ($\delta_a = -\delta_b = \delta$), as required by Eq. (2.46). To obtain the functions for α and the corresponding phase constraints, we follow the same procedure as in the undriven case. Rewriting the Hamiltonian H_d in the basis $\{\left|gg\right\rangle, \left|S\right\rangle, \left|T\right\rangle, \left|ee\right\rangle\}$, we get

$$\begin{aligned} H_d = \Big[& -i\beta S_R(\sqrt{\Gamma_{aR}^*} + \sqrt{\Gamma_{bR}^*})(\left|ee\right\rangle\left\langle T\right| + \left|T\right\rangle\left\langle gg\right|) \\ & -i\beta S_R(\sqrt{\Gamma_{aR}^*} - \sqrt{\Gamma_{bR}^*})(\left|ee\right\rangle\left\langle S\right| - \left|S\right\rangle\left\langle gg\right|)\Big] + \text{H.c.}. \end{aligned} \tag{2.54}$$

In the driven-dissipative regime, relaxation rates may vary with the propagation directions. Here, we set $\gamma_{nR} = \gamma_R$, $\gamma_{nL} = \gamma_L$, with the difference denoted by . The resulting constraints are summarized in Table B.2

If we take a closer look at Table B.1 and Table B.2, we find that the phase shifts in each topology should ensure that the individual relaxation rates are nonezero. Otherwise, the atom is not able to share the excitation or absorb the photon emitted by another atom. For the driven system, we perform numerical simulations in `Python` and present two figures (Fig. 2.6a and Fig. 2.6b) to study how the drive strength influences the formation of dark states. They show that as the drive increases, the dark states approach the Bell states $\left|S/T\right\rangle$, which are also maximally entangled states for two atoms. Moreover, Ref. [6] demonstrate that giant atoms can reach dark states faster than small atoms. The phase-shift arrangements during the simulation are listed in Table 2.2. We use the following equation to quantify the overlap between the dark states and the Bell states

$$\text{Overlap} = \left\langle S/T\right|\rho\left|S/T\right\rangle. \tag{2.55}$$

For clarity, numerical simulations given in this thesis follow a consistent normalization scheme. All frequency-related parameters are normalized to the relaxation rate γ. Consequently, the following dimensional relations hold:

$$\begin{aligned} & \delta_j \sim \gamma \sim \frac{1}{\text{time}}, \\ & |\beta|^2 \sim \text{time} \Rightarrow \beta \sim 1/\sqrt{\gamma}. \end{aligned} \tag{2.56}$$

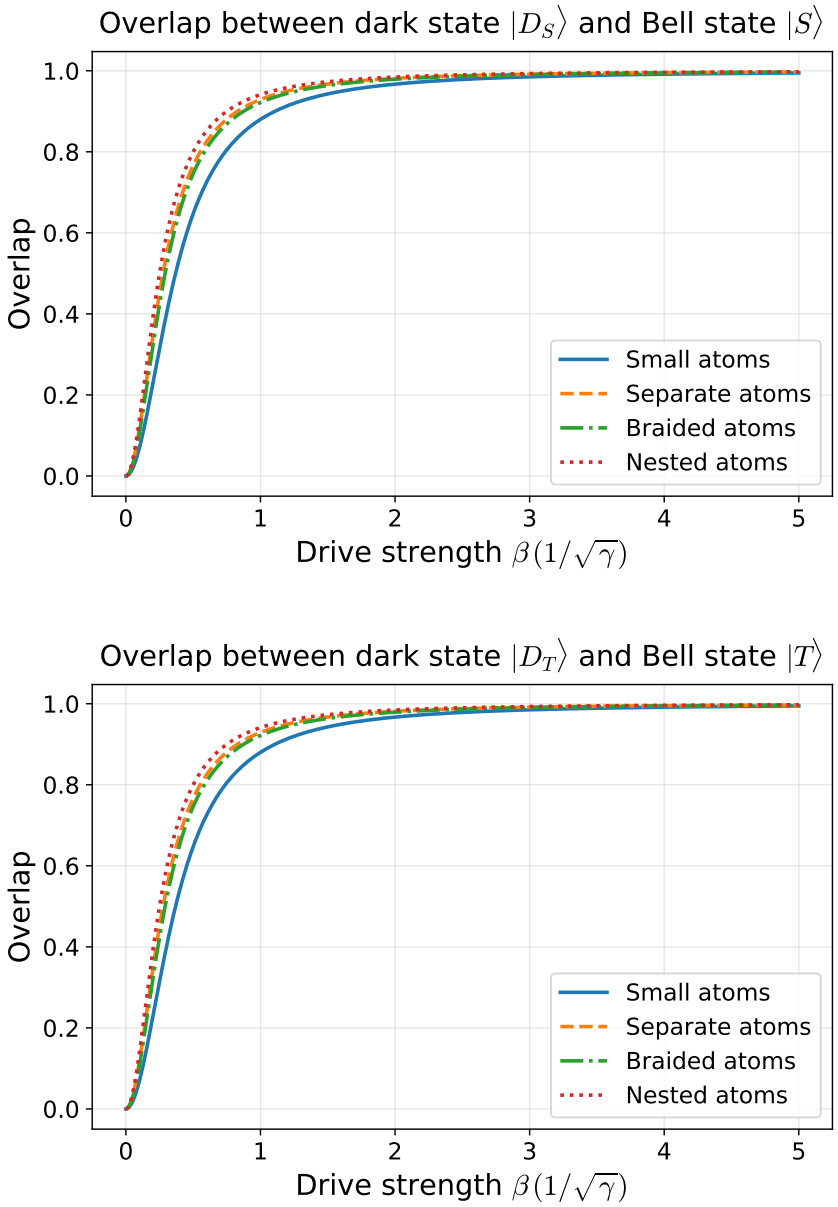

Figure 2.6: The drive-strength dependence of overlaps in the ideal waveguide. *Top*: the overlap between the $|D_S\rangle$ ans $|S\rangle$. *Bottom*: the overlap between the $|D_T\rangle$ and $|T\rangle$. In the Python code, we set $\delta = 0.5\gamma$, $\Delta_\gamma = 0.3\gamma$. Phase-shift settings are shown in Table 2.2.

Table 2.2: Phase-shift arrangements for the simulation of the dark states in driven-dissipative regime.

Topologies	Dark states	Phase shifts
Small	$\|D_S\rangle$	$\phi_1 = 0$
	$\|D_T\rangle$	$\phi_1 = \pi$
Separate	$\|D_S\rangle$	$\phi_1 = \phi_2 = \phi_3 = 0$
	$\|D_T\rangle$	$\phi_1 = \phi_3 = 0$
		$\phi_2 = \pi$
Braided	$\|D_S\rangle$	$\phi_1 = \phi_3 = 0$
		$\phi_2 = \frac{\pi}{2}$
	$\|D_T\rangle$	$\phi_1 = \phi_3 = \pi$
		$\phi_2 = \frac{\pi}{2}$
Nested	$\|D_S\rangle$	$\phi_1 = \phi_3 = 0$
		$\phi_2 = \frac{\pi}{2}$
	$\|D_T\rangle$	$\phi_1 = \phi_3 = \pi$
		$\phi_2 = \frac{\pi}{2}$

2.4 Giant atoms in a lossy waveguide

The method to describe the giant atoms in the lossy waveguide is also the SLH formalism. The first important question is how to model a lossy waveguide. In order to do this, beam splitters are inserted between neighboring coupling points [25], also the triplet of beam splitters and the SLH scheme are shown in the following content.

In the waveguides, quantum systems interact with the "non-guided" modes, which give rise to losses [25]. One usual way to model the loss is introducing a fictitious mode representing the non-guided modes [25]. Considering that photons are continuously lost along the propagation path, beam splitters with vacuum input are introduced to model the loss, where the reflection and transmission coefficients are

functions of the distance between neighboring coupling points.

The beam splitter is a component with two inputs and two outputs (Fig. 2.7). The triplet of beam splitter is

$$G_{bs} = \left(\begin{pmatrix} r_{11} & t_{12} \\ t_{21} & r_{22} \end{pmatrix}, \begin{pmatrix} 0 \\ 0 \end{pmatrix}, 0 \right). \tag{2.57}$$

where r and t represent the reflection and transmission coefficients, respectively. As Fig 2.7 shows, the reflected field is the output pairs of the input field. The first index after r and t labels the output port, while the second labels the input port. The scattering matrix also satisfies the unitary condition $\mathbf{S}_{bs}^{\dagger}\mathbf{S}_{bs} = I$. To simplify, we choose the beam-splitter scattering matrix in the following form

$$\mathbf{S}_{bs}^{n} = \begin{pmatrix} -i\sqrt{\varepsilon_n} & \sqrt{1-\varepsilon_n} \\ \sqrt{1-\varepsilon_n} & -i\sqrt{\varepsilon_n} \end{pmatrix}, \varepsilon \in \mathbb{R} \tag{2.58}$$

where n is the index of the beam splitter. Since the losses in the waveguide are extremely small and depend on the distance d, we introduce an attenuation coefficient f with units of inverse length (1/length). The total loss ε_n between two coupling points separated by a distance d_n is then given by

$$\varepsilon_n = 1 - e^{-fd_n} \ll 1, \tag{2.59}$$

which corresponds to the condition $fd_n \ll 1$. To account for the distributed loss along the waveguide, a beam splitter is introduced between each pair of coupling points.(Fig. 2.8a).

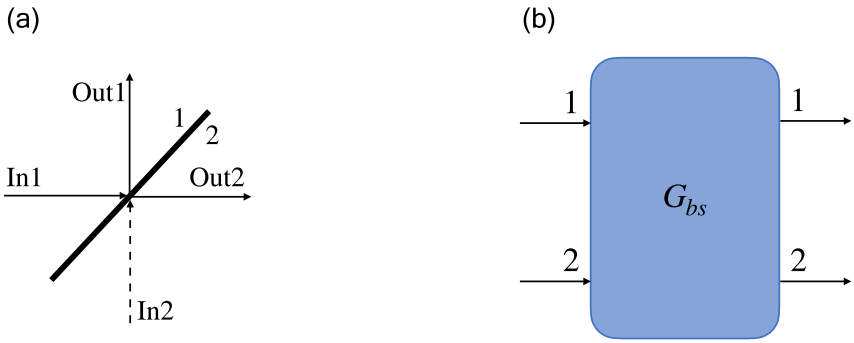

Figure 2.7: (a) For a bosonic stream propagating from left to right, this figure shows a beam splitter with inputs In1, In2 and outputs Out1, Out2, where In2 is vacuum input and Out1 accounts for photon loss. (b) The corresponding SLH scheme. Figures adapted from Refs. [25, 26].

Starting with a single giant atom coupled to the lossy waveguide in the undriven system, we remove the coherent drive β from the setup shown in Fig. 2.8a. Following the discussion in Sec. 2.3 and applying the SLH rules, the corresponding triplets for

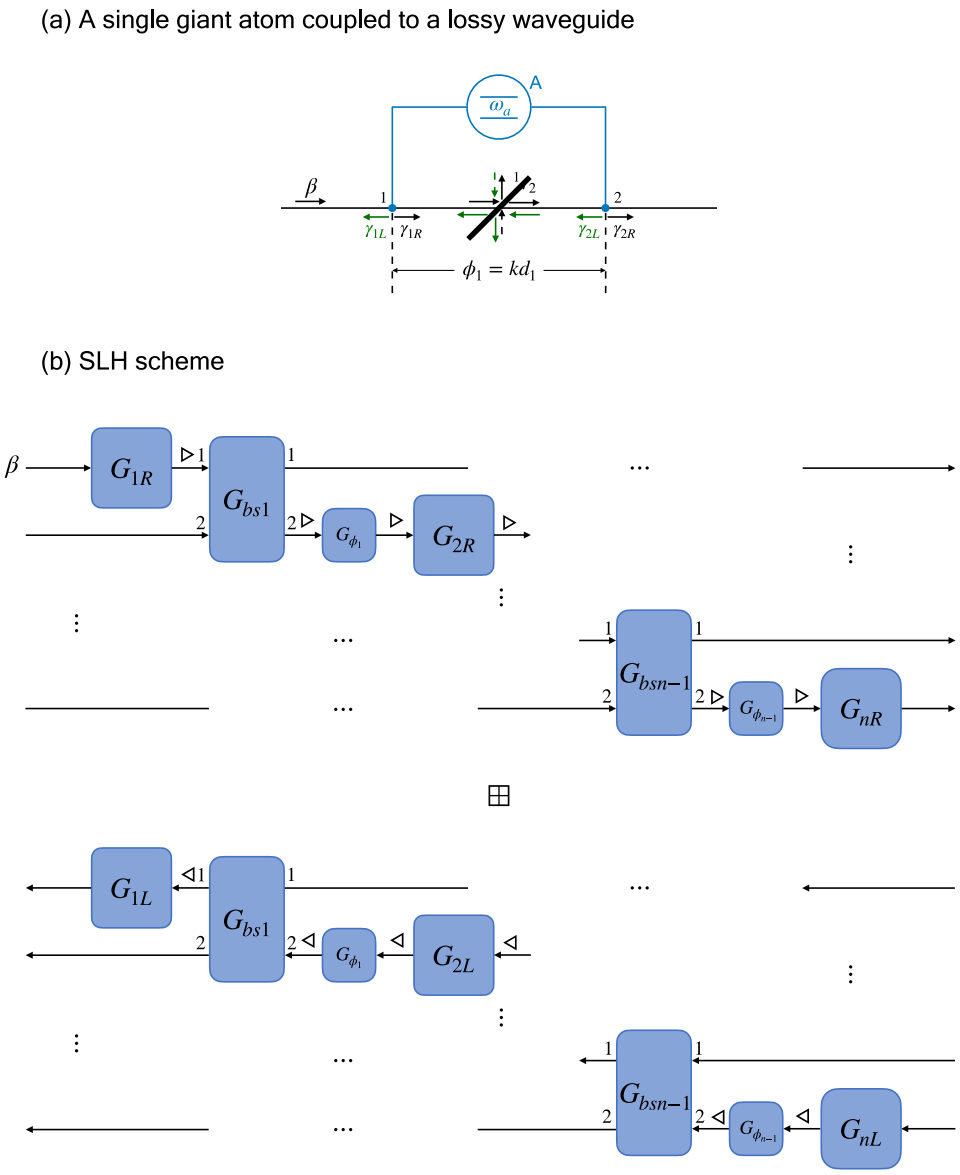

Figure 2.8: A single giant atom coupled to a lossy waveguide. These two figures show the driven system. We can also investigate the undriven system by just removing the drive. (a) A figure shows how to use a beam splitter to model a lossy waveguide, and this is a system with a coherent drive. The dark arrows represent the rightward propagating mode, and the leftward propagating mode is marked with green arrows. (b) A general SLH scheme for atoms coupled to a lossy waveguide with arbitrary coupling points.

this system are given by

$$\begin{aligned} G_R\Big|_{\text{loss}} &= (\mathbb{I} \boxplus (G_{2R} \lhd G_{\phi_1})) \lhd G_{bs1} \lhd (G_{1R} \boxplus \mathbb{I}) \\ &= \left(\begin{pmatrix} 1 & 0 \\ 0 & e^{i\phi_1} \end{pmatrix}, \begin{pmatrix} 0 \\ \sqrt{\gamma_{2R}}\sigma_-^a \end{pmatrix}, 0 \right) \lhd \left(\begin{pmatrix} r_{11}^1 & t_{12}^1 \\ t_{21}^1 & r_{22}^1 \end{pmatrix}, \begin{pmatrix} 0 \\ 0 \end{pmatrix}, 0 \right) \\ &\quad \lhd \left(\begin{pmatrix} 1 & 0 \\ 0 & 1 \end{pmatrix}, \begin{pmatrix} \sqrt{\gamma_{1R}}\sigma_a^- \\ 0 \end{pmatrix}, \frac{\omega_a}{2}\sigma_z^a \right), \end{aligned} \tag{2.60}$$

$$
\begin{aligned}
G_L\big|_{\text{loss}} &= (G_{1L} \boxplus \mathbb{I}) \triangleleft G_{bs1} \triangleleft (\mathbb{I} \boxplus (G_{\phi_1} \triangleleft G_{2L})) \\
&= \left(\begin{pmatrix} 1 & 0 \\ 0 & 1 \end{pmatrix}, \begin{pmatrix} \sqrt{\gamma_{1L}}\sigma_-^a \\ 0 \end{pmatrix}, 0 \right) \triangleleft \left(\begin{pmatrix} r_{11}^1 & t_{12}^1 \\ t_{21}^1 & r_{22}^1 \end{pmatrix}, \begin{pmatrix} 0 \\ 0 \end{pmatrix}, 0 \right) \\
&\quad \triangleleft \left(\begin{pmatrix} 1 & 0 \\ 0 & e^{i\phi_1} \end{pmatrix}, \begin{pmatrix} 0 \\ e^{i\phi_1}\sqrt{\gamma_{2L}}\sigma_-^a \end{pmatrix}, 0 \right),
\end{aligned}
\tag{2.61}
$$

where $\mathbb{I}$ is the identity triplets with an identity scattering matrix I to make sure the right connection. The resulting components are

$$
\begin{aligned}
\mathbf{S}_a\big|_{\text{loss}} &= \begin{pmatrix} r_{11}^1 & t_{12}^1 & 0 & 0 \\ e^{i\phi_1}t_{21}^1 & e^{i\phi_1}r_{22}^1 & 0 & 0 \\ 0 & 0 & r_{11}^1 & e^{i\phi_1}t_{12}^1 \\ 0 & 0 & t_{21}^1 & e^{i\phi_1}r_{22}^1 \end{pmatrix}, \\
\mathbf{L}_a\big|_{\text{loss}} &= \begin{pmatrix} \sqrt{\gamma_{1R}}r_{11}^1\sigma_-^a \\ \left(e^{i\phi_1}\sqrt{\gamma_{1R}}t_{21}^1 + \sqrt{\gamma_{2R}}\right)\sigma_-^a \\ \left(\sqrt{\gamma_{1L}} + e^{i\phi_1}\sqrt{\gamma_{2L}}t_{12}^1\right)\sigma_-^a \\ e^{i\phi_1}\sqrt{\gamma_{2L}}r_{22}^1\sigma_-^a \end{pmatrix}, \\
H_a\big|_{\text{loss}} &= \frac{\omega_a}{2}\sigma_z^a + \frac{1}{2i}\Big[\left(e^{i\phi_1}t_{21}^1 - e^{-i\phi_1}t_{21}^{1*}\right)\sqrt{\gamma_{1R}\gamma_{2R}} \\
&\quad + \left(e^{i\phi_1}t_{12}^1 - e^{-i\phi_1}t_{12}^{1*}\right)\sqrt{\gamma_{1L}\gamma_{2L}}\Big]\sigma_+^a\sigma_-^a.
\end{aligned}
\tag{2.62}
$$

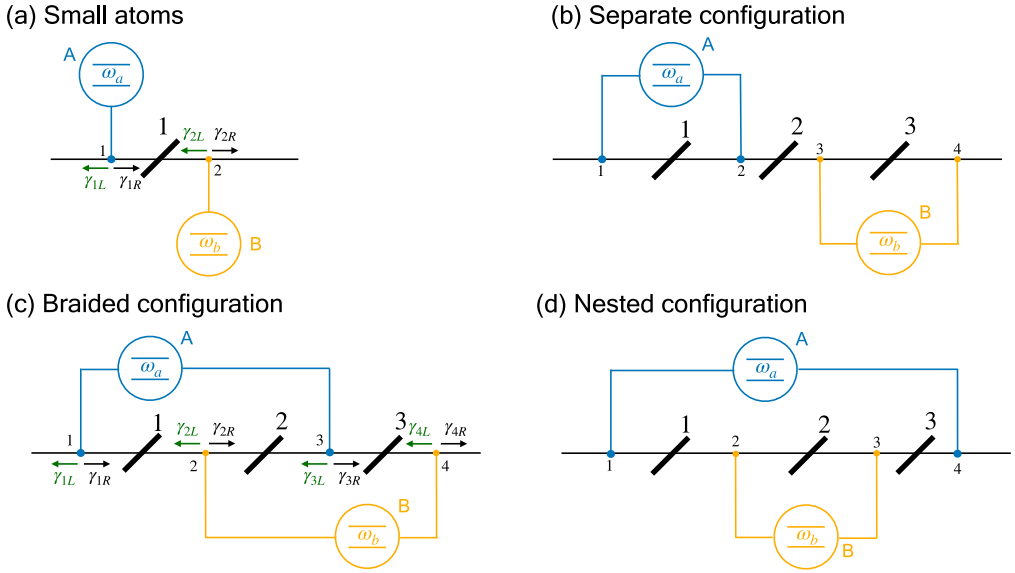

Figure 2.9: Two atoms coupled to a lossy waveguide. (a) Small atoms; (b–d) giant atoms in separate, braided, nested configuration.

Similarly, as an illustrative example for multiple atoms (Fig. 2.9), we consider

braided giant atoms, for which the right and left traveling triplets are

$$\begin{aligned} G_R\Big|_{\text{braided}}^{\text{loss}} =&(\mathbb{I}_3 \boxplus (G_{4R} \triangleleft G_{\phi_3})) \triangleleft (\mathbb{I}_2 \boxplus G_{bs3}) \triangleleft (\mathbb{I}_2 \boxplus (G_{3R} \triangleleft G_{\phi_2}) \boxplus \mathbb{I}) \\ &\triangleleft (\mathbb{I} \boxplus G_{bs2} \boxplus \mathbb{I}) \triangleleft (\mathbb{I} \boxplus (G_{2R} \triangleleft G_{\phi_1}) \boxplus \mathbb{I}_2) \\ &\triangleleft (G_{bs1} \boxplus \mathbb{I}_2) \triangleleft (G_{1R} \boxplus \mathbb{I}_3), \end{aligned} \tag{2.63}$$

$$\begin{aligned} G_L\Big|_{\text{braided}}^{\text{loss}} =&(G_{1L} \boxplus \mathbb{I}_3) \triangleleft (G_{bs1} \boxplus \mathbb{I}_2) \triangleleft (\mathbb{I} \boxplus (G_{\phi_1} \triangleleft G_{2L}) \boxplus \mathbb{I}_2) \\ &\triangleleft (\mathbb{I} \boxplus G_{bs2} \boxplus \mathbb{I}) \triangleleft (\mathbb{I}_2 \boxplus (G_{\phi_2} \triangleleft G_{3L}) \boxplus \mathbb{I}) \\ &\triangleleft (\mathbb{I}_2 \boxplus G_{bs1}) \triangleleft (\mathbb{I}_3 \boxplus (G_{\phi_3} \triangleleft G_{4L})). \end{aligned} \tag{2.64}$$

The results in some components are

$$\begin{aligned} \mathbf{S}_R\Big|_{\text{loss}} &= \begin{pmatrix} \mathbf{S}_{R1} & \mathbf{S}_{R2} & \mathbf{S}_{R3} & \mathbf{S}_{R4} \end{pmatrix}, \\ \mathbf{L}_R\Big|_{\text{loss}} &= \begin{pmatrix} L_{R1} \\ L_{R2} \\ L_{R3} \\ L_{R4} \end{pmatrix} \end{aligned} \tag{2.65}$$

$$\begin{aligned} \mathbf{S}_L\Big|_{\text{loss}} &= \begin{pmatrix} \mathbf{S}_{L1} & \mathbf{S}_{L2} & \mathbf{S}_{L3} & \mathbf{S}_{L4} \end{pmatrix}, \\ \mathbf{L}_L\Big|_{\text{loss}} &= \begin{pmatrix} L_{L1} \\ L_{L2} \\ L_{L3} \\ L_{L4} \end{pmatrix}. \end{aligned} \tag{2.66}$$

Then the final results are

$$\begin{aligned} \mathbf{S}\Big|_{\text{loss}} &= \begin{pmatrix} \mathbf{S}_R & 0 \\ 0 & \mathbf{S}_L \end{pmatrix}, \\ \mathbf{L}\Big|_{\text{loss}} &= \begin{pmatrix} \mathbf{L}_R \\ \mathbf{L}_L \end{pmatrix}, \\ H\Big|_{\text{loss}} &= H_R + H_L \\ &= \frac{\omega_a'}{2}\sigma_z^a + \frac{\omega_b'}{2}\sigma_z^b + g\sigma_-^a\sigma_+^b + g^*\sigma_-^a\sigma_+^b. \end{aligned} \tag{2.67}$$

With the triplets above, the Lindblad master equation can also be extracted in the form Eq. (2.44).

If a coherent drive is added in the waveguide, the triplet of the left-traveling mode keeps the same, the right-traveling mode triplet has extra terms

$$\mathbf{L}_d\Big|_{\text{loss}} = \begin{pmatrix} L_{d1} \\ L_{d2} \\ L_{d3} \\ L_{d4} \end{pmatrix} = \begin{pmatrix} \beta r_{11}^1 \\ e^{i\phi_1}\beta t_{21}^1 \\ e^{i(\phi_1+\phi_2)}\beta t_{21}^1 t_{21}^2 r_{11}^3 \\ e^{i(\phi_1+\phi_2+\phi_3)}\beta t_{21}^1 t_{21}^2 t_{21}^3 \end{pmatrix} \tag{2.68}$$

$$H_{\text{drive}}\Big|_{\text{loss}} = \frac{1}{2i}[\beta \mathbf{L}_R^\dagger \mathbf{S}_{R1} - \text{H.c.}] \tag{2.69}$$

Similarly to atoms coupled to an ideal waveguide, expanding the master equation with the extra terms above, the dynamics of the system is the same as the system with the master equation in the following

$$\dot{\rho} = -i[H_u + H_d, \rho] + \sum_m \mathcal{D}[L_{Rm}]\rho + \sum_m \mathcal{D}[L_{Lm}]\rho, \tag{2.70}$$

where the equation of H_d is

$$H_d\Big|_{\text{loss}} = -i\beta \mathbf{L}_R^\dagger \mathbf{S}_{R1} + \text{H.c.} \tag{2.71}$$

With this form of master equation, the calculation will be easier.

In the lossy waveguide, the Hamiltonian H_u has the same general form as Eq. (2.47), with modified parameter expressions. Together with the results for the other topologies presented in Appendix C, this provide the basis for discussing the individual and collective relaxation rates in the next chapter.

3

Results

Building upon the theoretical framework and derivations established in the previous chapter, this chapter shows the impacts of two primary imperfections: asymmetric coupling and lossy waveguides. The core of this research evaluates the stability of decoherence-free interaction and dark states under these non-ideal conditions. We demonstrate that DFI and dark states are destroyed under these imperfections. Furthermore, we provide a quantitative analysis of the shifts in decoherence-suppression mechanisms and establish the bounds for waveguide losses.

3.1 Symmetric and asymmetric couplings

3.1.1 A single giant atom

This section begins with an analysis of a single-atom system. In the symmetric case ($\gamma_{1R/L} = \gamma_{2R/L} = \gamma$), the effective relaxation rate Γ_a of a single giant atom vanishes when the distance between coupling points is an odd multiple of half wavelengths. However, in the asymmetric case, an imperfection characterized by unequal bare relaxation rates from the same atom, i.e., $\gamma_{1R/L} = \epsilon\gamma_{2R/L} = \epsilon\gamma$ (where $0 < \epsilon < 1$), the relaxation rate is given by:

$$\Gamma_a = 2\gamma(\epsilon + 1 + 2\sqrt{\epsilon}\cos kd_1). \tag{3.1}$$

As illustrated in Eq. (3.1) and Fig. 3.1, the decoherence protection is lifted in the asymmetric case, as evidenced by a vertical shift at the previous decoherence-free point. The magnitude of this shift is expressed as:

$$\delta_{\Gamma_a} = 2\gamma(1 + \epsilon - 2\sqrt{\epsilon}). \tag{3.2}$$

Furthermore, this shift is not confined to the decoherence-free point but exists across nearly all phase-shift cases. According to Eq. (3.1), the impact from asymmetry is periodic.

3.1.2 Braided atoms

In the symmetric case of braided atoms, as detailed in Sec. 2.3.3.1 and Table. 2.1, decoherence-free interaction occurs when the distances between coupling points for each atom satisfies the half wavelength, i.e., $d_1+d_2 = d_2+d_3 = \lambda/2$. Given that DFI

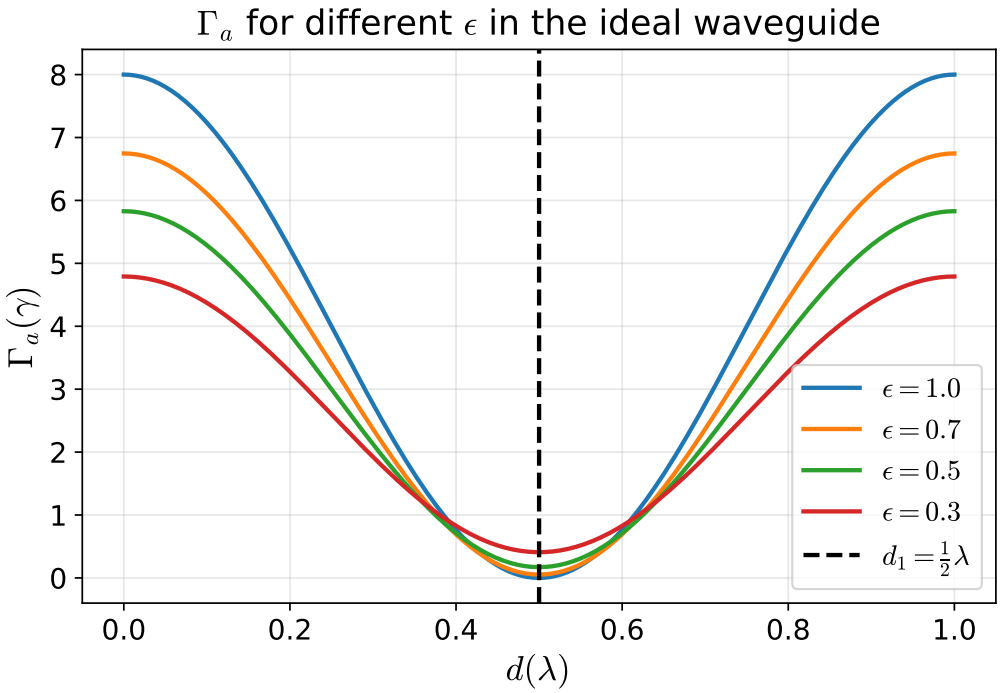

Figure 3.1: Effective relaxation rate under asymmetric coupling conditions. The parameter ϵ represents the ratio of the bare relaxation rates γ_1/γ_2. The dark line $d_1 = \lambda/2$ indicates that the system is protected from decoherence for the symmetric case ($\epsilon = 1$). In the asymmetric case ($\epsilon < 1$), the minimum relaxation rate exhibits a vertical shifts away from the decoherence-free point. Different colors denote various coupling ratios ϵ.

represents one of the most interesting phenomena in the two-giant-atom system, our discussion of asymmetric coupling focuses exclusively on the braided configuration.

In the asymmetric case of the braided atoms, the arrangement of bare relaxation rates are $\gamma_{1R/L} \neq \gamma_{3R/L}$, $\gamma_{2R/L} \neq \gamma_{4R/L}$. To simplify, we assume $\gamma_{1R/L} = \gamma_{2R/L} = \epsilon\gamma$, $\gamma_{3R/L} = \gamma_{4R/L} = \gamma$, then exchange interaction, individual and collective relaxation rates yield

$$\begin{aligned}
\Gamma_a &= 2\gamma(\epsilon + 1 + 2\sqrt{\epsilon}\cos k(d_1 + d_2)), \\
\Gamma_b &= 2\gamma(\epsilon + 1 + 2\sqrt{\epsilon}\cos k(d_2 + d_3)), \\
\Gamma_{\text{coll}} &= 2\gamma[\epsilon\cos kd_1 + \sqrt{\epsilon}\cos kd_2 + \cos kd_3 + \sqrt{\epsilon}\cos k(d_1 + d_2 + d_3)], \\
g &= \gamma[\epsilon\sin kd_1 + \sqrt{\epsilon}\sin kd_2 + \sin kd_3 + \sqrt{\epsilon}\sin k(d_1 + d_2 + d_3)].
\end{aligned} \tag{3.3}$$

As shown in Eq. (3.3), the individual relaxation rate Γ_j cannot be zero, when $0 < \epsilon < 1$. In our Python code, we set $d_n = d$. At the specific configuration where $d_1 + d_2 = d_3 + d_4 = \lambda/2$, Fig. 3.2 reveals an offset in the individual relaxation rates; specifically, the minimum individual relaxation rate is given by $\Gamma_{a/b}|_{\min} = 2\gamma(1 - \sqrt{\epsilon})^2$, while the collective relaxation rate vanishes. As the asymmetry decreases ($\epsilon \to 1$), this minimum value approaches zero, restoring the ideal suppressed decay. Additionally, Fig. 3.2 illustrates that an ϵ closer to 1 enhances the coupling strength.

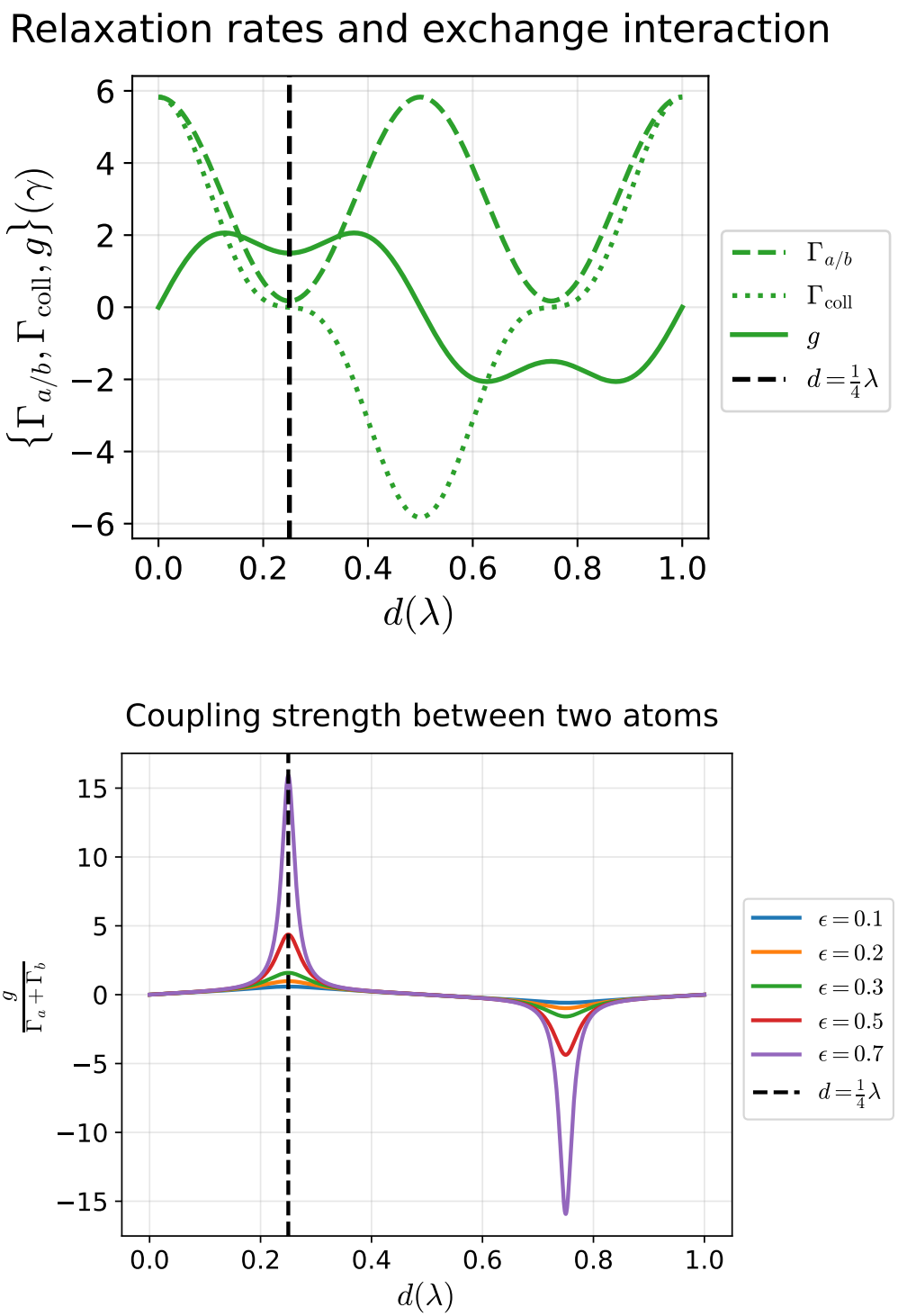

Figure 3.2: *Top*: Relaxation rates and exchange interaction in a system of braided atoms with asymmetric coupling to an ideal waveguide, and parameter ϵ used in python code is $\epsilon = 0.5$. *Bottom*: Coupling strength between atoms relative to individual relaxation rates. The parameter $d_n = d$ is assumed for both cases.

3.2 DFI in lossy waveguides

3.2.1 A single giant atom

For a single giant atom coupled to a lossy waveguide, by substituting the jump operators from Eq. (2.62) into the definition of the master equation, we get the relaxation rate:

$$\Gamma_a = \gamma_{1R} + \gamma_{2R} + \gamma_{1L} + \gamma_{2L} + 2(\sqrt{\gamma_{1R}\gamma_{2R}} + \sqrt{\gamma_{1L}\gamma_{2L}})\cos(kd_1)\sqrt{1-\varepsilon_1}, \tag{3.4}$$

where $\varepsilon_1 = 1 - e^{-fd_1}$ represents the total losses. In the limit of extremely low losses ($fd_1 \ll 1$) and assuming symmetric couplings, i.e., $\gamma_{nR/L} = \gamma$, the equation yields to the following first-order approximation:

$$\Gamma_a \approx 4\gamma[1 + (1 - \frac{1}{2}fd_1)\cos kd_1]. \tag{3.5}$$

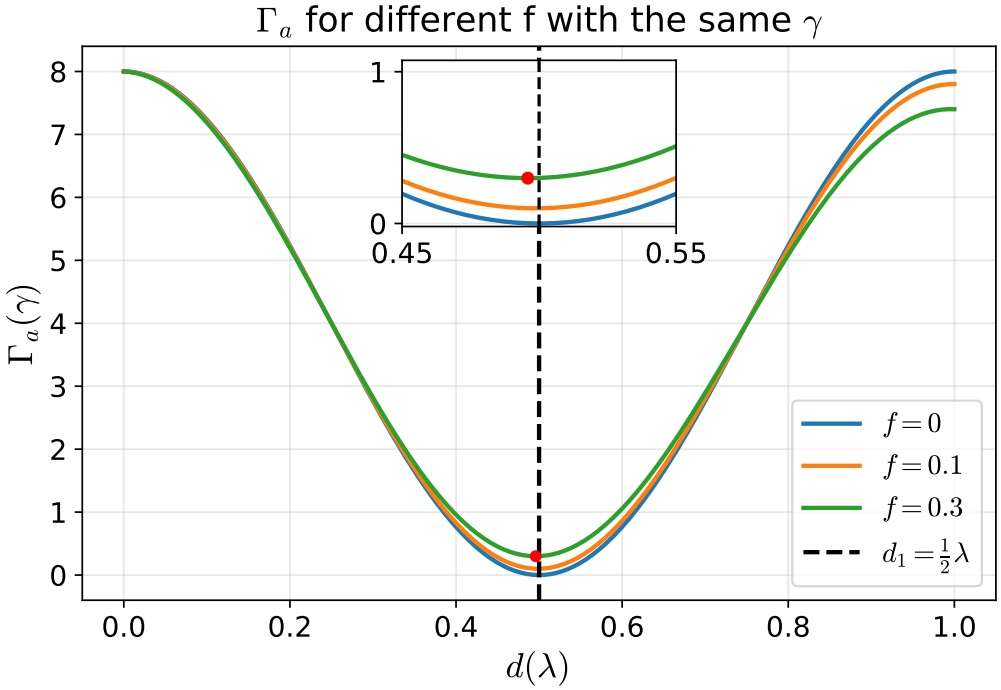

Figure 3.3: Individual relaxation rate under different losses. Here f is referred an attenuation coefficient. The dark line $d_1 = \lambda/2$ corresponds to a decoherence-free point for a single giant atom coupled to the ideal waveguide. In the presence of loss, the minimum relaxation rate both vertical and horizontal shifts away from the decoherence-free point. Specifically, for the green line ($f = 0.3(1/\text{length})$), the red point identifies the smallest effective relaxation rate for atom a. The inset at the top center provides a magnified view of the region around the minimum point.

Fig. 3.3 illustrate the behavior of Eq. (3.5) as plotted using `Python`. It shows horizontal and vertical shifts from the line $d_1 = \lambda/2$, indicating that the interference mechanism protecting the system from decoherence is destroyed by waveguide losses.

To quantify these deviations, we denote the horizontal and vertical shifts as δ_d and δ_{Γ_a}, respectively. By applying applying a *Taylor expansion* to the first derivation of Eq. (3.5) around the ideal decoherence-free point, we obtain:

$$\frac{\mathrm{d}\Gamma_a}{\mathrm{d}d_1} = 2\gamma[f + k^2(2 - \frac{\lambda}{2}f)\delta_d]. \tag{3.6}$$

Setting $\frac{\mathrm{d}\Gamma_a}{\mathrm{d}d_1} = 0$ to find the minimum relaxation rate, we derive the following shifts:

$$\begin{aligned} \delta_d &\approx -\frac{f}{2k^2} + \mathcal{O}(f^2), \\ \delta_{\Gamma_a} &\approx \frac{2\pi f\gamma}{k} = 2\gamma f d_1 = 2\gamma\varepsilon_1. \end{aligned} \tag{3.7}$$

Comparing the vertical shift δ_{Γ_a} to the maximum individual relaxation rate $\Gamma_a|_{\max} = 8\gamma$ shown in Fig. 3.3, we then get the following ratio:

$$\frac{\delta_{\Gamma_a}}{\Gamma_a|_{\max}} = \frac{\varepsilon_1}{4} \ll 1. \tag{3.8}$$

Under the constraints of $\epsilon_1 \ll 1$, a single atom's decoherence protection is resilient, ensuring that the dynamics of system are not significantly influenced by extremely minor waveguide losses.

In the previous calculation we use following Taylor expansions: $\sin x$, $\cos x$, $1/(1-x)$, e^x. Because of the extremely small losses and shifts observed in practice, only the first-order approximation is retained during the derivation.

Then another critical issue is the upper bound of losses. In order to address this, we look into an experiment in Ref. [5], where a superconducting qubit is coupled to a one-dimensional microwave transmission line at two discrete locations. According to the data in Ref. [5], for the single qubit, the minimum effective relaxation rate and the bare relaxation rates are given by:

$$\begin{aligned} \delta_{\Gamma_a} &= \Gamma_a\Big|_{d_1=\frac{\lambda}{2}} = 1/T_a = 1/31.5\mu s \approx 0.03\text{MHz}, \\ \gamma_n &= 2\gamma = 2\text{MHz}, \end{aligned} \tag{3.9}$$

where $T_a = 31.5\mu s$ is the measured relaxation time. From these values, total losses can be estimated as $\varepsilon_1 = \delta_d/\gamma_n = 0.015$. Consequently, the attenuation coefficient should not be greater than the following upper bound:

$$f = \frac{2\varepsilon_1}{\lambda} = 0.03/\lambda. \tag{3.10}$$

It should be noted that the realistic lossy mechanisms are highly complicated, this study focuses exclusively on waveguide-induced losses that depend on the distance. In most experiments, including the single-qubit demonstration in Ref. [5], the phase shift is typically tuned by changing the qubit frequencies. Verifying whether the

point of minimum relaxation rate coincides with the half-wavelength condition requires exact knowledge of both the physical distance between coupling points and the velocity of bosonic field. However, simultaneously determining these parameters with high precision remains a significant challenge, making it difficult to directly identify the loss-induced horizontal shift in such experimental setups. Nevertheless, according to Eq. (3.7), if a horizontal shift were to manifest in this experiment, its theoretical value is estimated to be around $-0.015/(2\pi k)$.

When a single giant atom is asymmetrically coupled to a lossy waveguide, we assume left-right symmetric decay for each coupling point, i.e., $\gamma_{nR/L} = \gamma_{nR/L} = \gamma_n/2$. By introducing the asymmetry ratio $\epsilon = \gamma_1/\gamma_2 = 2\epsilon\gamma$, the effective individual relaxation rate of the giant atom can be derived as:

$$\Gamma_a = 2\gamma[1 + \epsilon + 2\sqrt{\epsilon(1-\varepsilon_1)}\cos kd_1]. \tag{3.11}$$

Consequently, the vertical shift of the minimum effective relaxation rate is given by:

$$\delta_{\Gamma_a} = 2\gamma[1 + \epsilon + 2\sqrt{\epsilon}(-1 + \frac{f\pi}{2k})]. \tag{3.12}$$

As discussed in Sec. 3.1.1, the asymmetric coupling primarily affects the vertical shift of the relaxation rate. Therefore, even in the asymmetric case, the horizontal shift δ_d caused by losses remains following Eq. (3.7). From the observed vertical and horizontal shifts, the two imperfections can be determined as follows:

$$\begin{aligned} f &= -2k^2\delta_d, \\ \epsilon &= \frac{\gamma_1}{\gamma_2} = \left(1 + \delta_d k\pi - \sqrt{(\delta_d\pi k)^2 + 2\delta_d\pi k + \frac{\delta_{\Gamma_a}}{2\gamma}}\right)^2. \end{aligned} \tag{3.13}$$

3.2.2 Multiple giant atoms

By referring to the general results in Appendix C and assuming symmetric coupling $\gamma_{nR/L} = \gamma$ with equal distance $d_n = d$, we obtain the specific parameters for two atoms coupled to a lossy waveguide as listed in the following Table 3.1:

Table 3.1: Frequency shifts, exchange interactions, individual and collective relaxation rates in the lossy waveguide. We set identical bare relaxation rates $\gamma_{nR/L} = \gamma$ and distance between neighboring coupling points $d_n = d$, and f is the attenuation coefficient.

Parameters	Topologies	Expressions
Frequency shifts (δ_{ω_a}, δ_{ω_b})	Small	0
	Separate	$2\gamma(1 - \frac{1}{2}fd)\sin kd$
	Braided	$2\gamma(1 - fd)\sin 2kd$

Continued on next page

Table 3.1 – continued from previous page

Parameters	Topologies	Expressions
	Nested	$2\gamma(1-\frac{3}{2}fd)\sin 3kd$
		$2\gamma(1-\frac{1}{2}fd)\sin kd$
Individual relaxation rates (Γ_a, Γ_b)	Small	2γ
	Separate	$4\gamma+4\gamma(1-\frac{1}{2}fd)\cos kd$
	Braided	$4\gamma+4\gamma(1-fd)\cos 2kd$
	Nested	$4\gamma+4\gamma(1-\frac{3}{2}fd)\cos 3kd$
		$4\gamma+4\gamma(1-\frac{1}{2}fd)\cos kd$
Collective relaxation rates (Γ_{coll})	Small	$2\gamma(1-\frac{1}{2})\cos kd$
	Separate	$2\gamma[(1-\frac{1}{2}fd)\cos kd+2(1-fd)\cos 2kd$
		$+(1-\frac{3}{2}fd)\cos 3kd]$
	Braided	$2\gamma[3(1-\frac{1}{2}fd)\cos kd+(1-\frac{3}{2}fd)\cos 3kd]$
	Nested	$2\gamma[2(1-\frac{1}{2}fd)\cos kd+2(1-fd)\cos 2kd]$
Exchange interactions (g)	Small	$\gamma(1-\frac{1}{2}fd)\sin kd$
	Separate	$\gamma[(1-\frac{1}{2}fd)\sin kd+2(1-fd)\sin 2kd$
		$+(1-\frac{3}{2}fd)\sin 3kd]$
	Braided	$\gamma[3(1-\frac{1}{2}fd)\sin kd+(1-\frac{3}{2}fd)\sin 3kd]$
	Nested	$\gamma[2(1-\frac{1}{2}fd)\sin kd+2(1-\frac{1}{2}fd)\sin 3kd]$

To more conveniently observe the results, Fig. 3.4 illustrates the exchange interactions, individual and collective relaxation rates for two atoms coupled to the lossy waveguide.

Fig. 3.4 shows that at $d = \lambda/4$ point, which corresponds to the decoherence-free interaction point (Fig. 2.4) for braided atoms coupled to an ideal waveguide, the individual relaxation rate does not vanish. Instead, a residual individual relaxation rate appears due to losses, given by

$$\Gamma_{a/b}\Big|_{d=\frac{\lambda}{4}} = \frac{2\pi\gamma f}{k} = 4\gamma fd = 4\gamma\varepsilon. \tag{3.14}$$

In contrast, the collective relaxation rate Γ_{coll} remains zero. This is consistent with a phenomenon of *subradiance* [12, 13, 33], where collective interference suppresses spontaneous emission, leading to a slower relaxation than that of each individual atom.

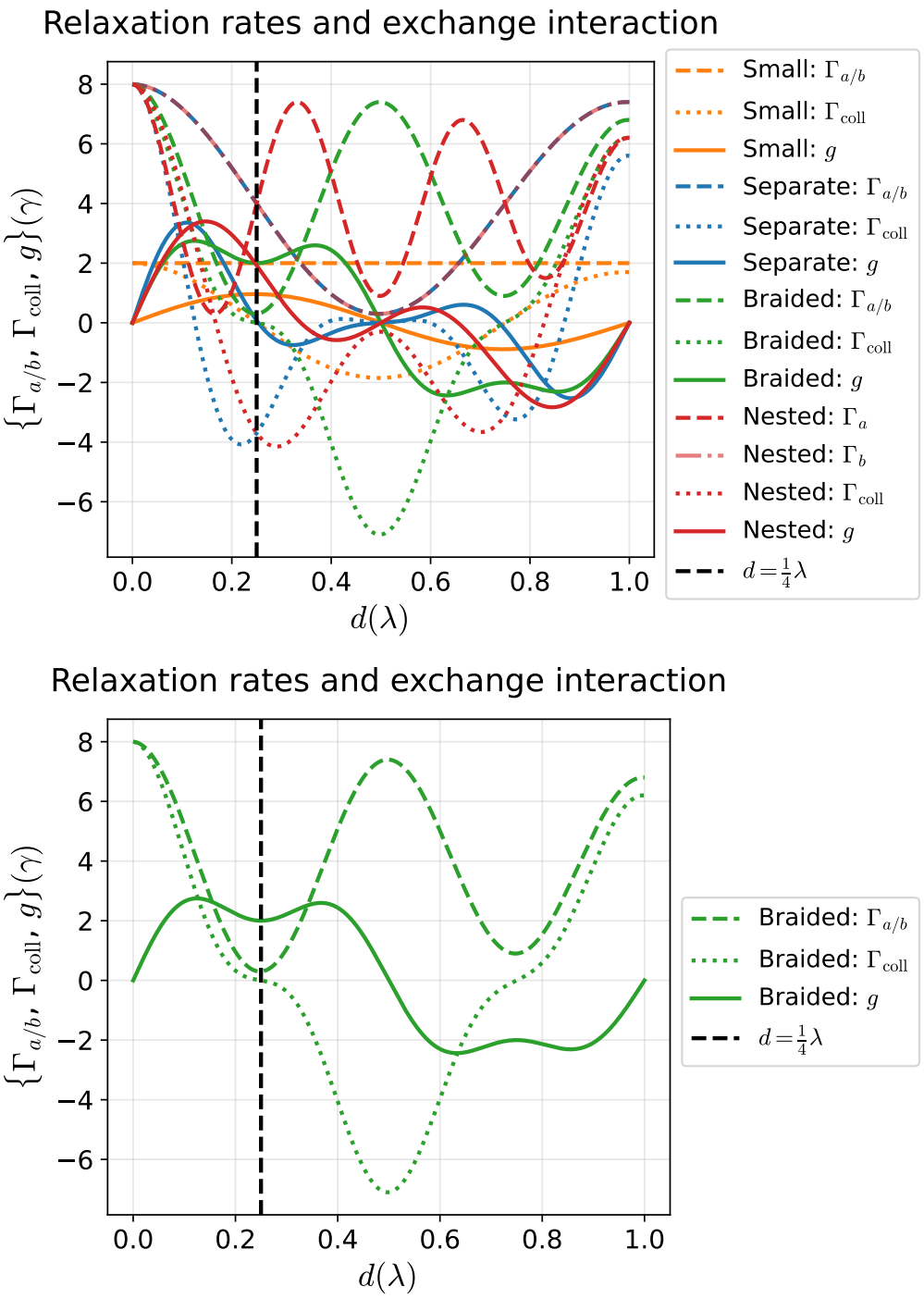

Figure 3.4: Comparison of relaxation rates and exchange interaction across all atomic topologies in a lossy waveguide. The dark vertical line ($d = \lambda/4$) marks the decoherence-free interaction distance in the ideal waveguide. *Top*: Results for small, separate, braided and nested atoms are represented by orange, blue, green and red curves, respectively. *Bottom*: Separately extracted braided configuration diagram. We focus primarily on the braided configuration in the lossy waveguide, where the individual relaxation rate is none-zero at a quarter wavelength, while the collective relaxation rate vanishes and the exchange interaction is reaches approximately 2γ. A attenuation coefficient of $f = 0.1/(1/\text{length})$ is assumed during the numerical simulations.

Comparing the minimum value (vertical shift) $\Gamma_{a/b}\Big|_{d=\frac{\lambda}{4}}$ to the maximum value $\Gamma_{a/b}\Big|_{\max} = 8\gamma$, we obtain the following relation:

$$\frac{\Gamma_{a/b}\Big|_{d=\frac{\lambda}{4}}}{\Gamma_{a/b}\Big|_{\max}} = \frac{\varepsilon}{2}. \tag{3.15}$$

Given that $\varepsilon \ll 1$, this ratio remains extremely small, confirming the robustness of DFI in the presence of minor losses.

Comparing the results discussed above, both DFI in braided atoms and decoherence free in a single giant atom are destroyed. This is because the individual relaxation rates no longer vanish under the joint influence of these two imperfections. Specifically, asymmetric coupling induces a periodic vertical shift in the relaxation rate. In addition, waveguide losses introduce an extra horizontal displacement from the decoherence-free point, as losses effects are cumulative with bosonic propagation distance.

3.3 Dark states in lossy waveguides

We now discuss the properties of the dark states in both undriven and driven systems. As a *perfectly subradiant state*, the formal restrictions for a dark state are established in Sec. 2.3.3.2.

In the quantum system coupled to a lossy waveguide, however, the jump operators include total dissipative channels that prevent the system from reaching a state that is strictly annihilated by these operators. Specifically, within the jump-operator matrix, the reflection coefficient r should be zero to satisfy the condition shown in Eq. (2.45). This requirement is fundamentally incompatible with the presence of propagation losses in the waveguide, as loss implies a non-zero attenuation that disrupts the perfect cancellation required for subradiance.

3.3.1 Undriven systems

In the lossy waveguide, the system state cannot become completely "dark," causing any initial state to eventually decay to the ground state $|gg\rangle$. The instantaneous spontaneous relaxation rate of the state $|S/T\rangle$ is defined as:

$$\Gamma_{S/T} = \sum_m \langle S/T| L_{Rm}^\dagger L_{Rm} |S/T\rangle + \sum_m \langle S/T| L_{Lm}^\dagger L_{Lm} |S/T\rangle . \tag{3.16}$$

Given that losses per distance are sufficiently small, we retain only the first-order terms when simplifying the expression for decay rate $\Gamma_{S/T}$. For small atoms, the relaxation rate is approximated as $\Gamma_{S/T} \approx \gamma f d_1$.

Based on the phase-shift configurations in Table B.1, the arrangements of the distances between the coupling points can be determined. Table 3.2 summarizes the

distance arrangements and the corresponding relaxation rates for all configurations. These results are valid under the reality of extremely low waveguide loss, and the assumption of $\gamma_{nR} = \gamma_{nL} = \gamma$. In this regime, the triplet state $|T\rangle$ performs a more stable entanglement. Notably, the relaxation rates for braided and nested configurations primarily depend on the attenuation coefficient and transition frequency.

Table 3.2: Distance arrangements between coupling points and instantaneous spontaneous relaxation rates $\Gamma_{S/T}$ for giant-atom systems. We assume equal bare relaxation rates at each coupling point n, with $\gamma_{nR} = \gamma_{nL} = \gamma$. For all configurations, the transition frequencies of of atom a and b are identical ($\omega_a = \omega_b = \omega$).

Configurations	States	Distances	Relaxation rates
Separate	$\|S\rangle$	$d_1 = d_3 = d \neq \frac{\lambda}{2}$ $d_2 = -d + \lambda > 0$	$2\gamma f(\lambda \cos kd + \lambda - d\cos kd)$
	$\|T\rangle$	$d_1 = d_3 = d \neq \frac{\lambda}{2}$ $d_2 = \frac{\lambda}{2} - d > 0$	$\gamma f(\lambda \cos kd + \lambda - 2d\cos kd)$
Braided	$\|S\rangle$	$d_1 = d_3 = \lambda$ $d_2 = d$	$2\gamma f\lambda$
	$\|T\rangle$	$d_1 = d_3 = \frac{\lambda}{2}$ $d_2 = d$	$\gamma f\lambda$
Nested	$\|S\rangle$	$d_1 = d_3 = \lambda$ $d_2 = d$	$2\gamma f\lambda$
	$\|T\rangle$	$d_1 = d_3 = \frac{\lambda}{2}$ $d_2 = d$	$\gamma f\lambda$

3.3.2 Coherently driven systems

In this complex system, the final state can be obtained by solve the following equation:

$$\dot{\rho} = -i[H_u + H_d, \rho] + \sum_m \mathcal{D}[L_{Rm}]\rho + \sum_m \mathcal{D}[L_{Lm}]\rho = 0, \tag{3.17}$$

with the constraint

$$\mathrm{Tr}\rho = 1. \tag{3.18}$$

With the Hamiltonians and jump operators obtained from the SLH formalism, we can get the matrix of the master equation. Two atoms provide a 4×4 matrix, leading

to a total of seventeen equations, which are too complicated to solve analytically. However, we can use `Python` to get numerical solutions.

In the ideal waveguide, the final states in the driven-dissipative regime are pure steady states, therefore, overlap with Bell states can be used to measure entanglement. In the lossy waveguide, the drive keeps exciting the system, while the losses randomly remove the excitation. Because these losses are stochastic and unobserved, the system evolves into a separable state. Under this situation, overlap is not a sufficient metric for measuring entanglement. We introduce *concurrence* to quantify the entanglement, which ranges from zero for separable states to one for maximally entangled states. This allows us to characterize how the drive affects the formation and degradation of entanglement.

Figs. 3.5–3.8 are generated by independently tuning the drive strength β or the attenuation coefficient f. The simulations adopt a uniform configuration, where $\gamma_{nL} = \gamma_L$, $\gamma_{nR} = \gamma_R$, and define the parameters as $\Delta_\gamma = \gamma_L - \gamma_R = 0.3\gamma$, $\delta_a = -\delta_b = \delta = 0.5\gamma$.

To ensure a fair comparison with the separate-atom system, we adjust the coupling point distances in the small-atom system to match those of the separate example. The results for separate atoms, illustrated in Fig. 3.6, confirm that the giant-atom system maintains a slightly advantage, including wider tolerance and generally higher peak values for both overlap and concurrence.

As shown in the left panels of Figs. 3.5–3.8, the overlap exhibits a trajectory similar to that of the concurrence before reaching their respective peaks with increasing drive strength. In an ideal waveguide (Fig. 2.6), regardless of the topology, the overlap approaches 1 and remains stable as the drive increases. In contrast, the results for a lossy waveguide (Fig. 3.5–3.8) reveal that further increasing the drive strength beyond these maxima causes both concurrence and overlap to decline. This indicates a transition toward a separable states, where quantum coherence is lost and the concurrence eventually vanishes. Also according to the numerical result, $\mathrm{Tr}\rho^2 < 1$, implying that the final state is mixed. All in all, in the strongly driven regime, the final state of the system is a separable mixed state.

From a experimental perspective, we define the tolerance for generating a high-fidelity entangled state as the range of loss coefficients where both overlap and concurrence remain above 0.8. Under a fixed drive strength, the specific tolerances for generating $|D_S\rangle$ and $|D_T\rangle$ are shown in figures.

The distance arrangements in Figs. 3.5–3.8 are governed by the phase shits detailed in Table. B.2. Utilizing braided atoms under a weak coherent drive to generate the state $|D_T\rangle$ is the best choice for achieving a “darker” entangled state, as the specific distance arrangement in this case minimizes the total propagation distance.

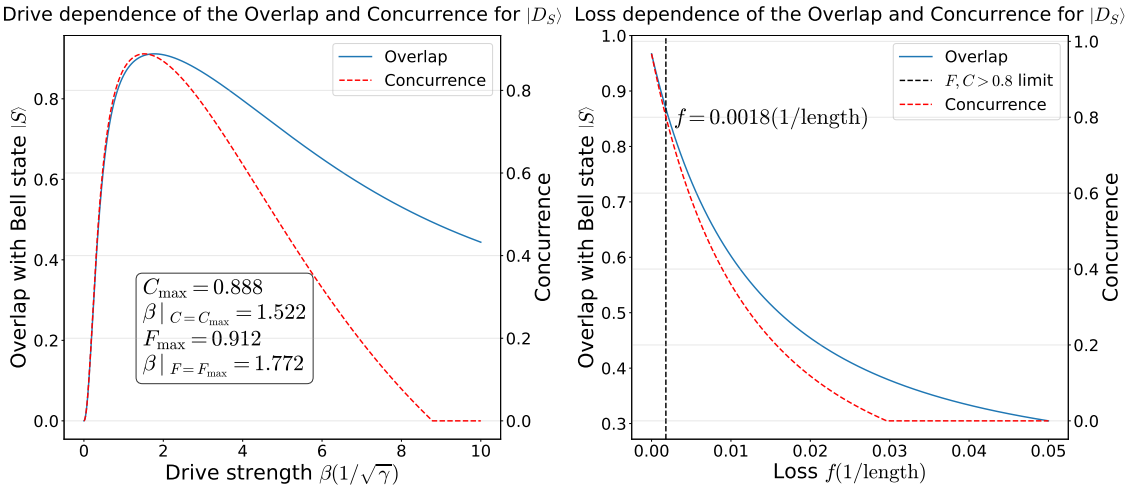

(a) Parameters: $d_S = 3\lambda$. Depending on the variable, we fix $f_{\text{fixed}} = 0.001(1/\text{length})$ or $\beta_{\text{fixed}} = 2/\sqrt{\gamma}$.

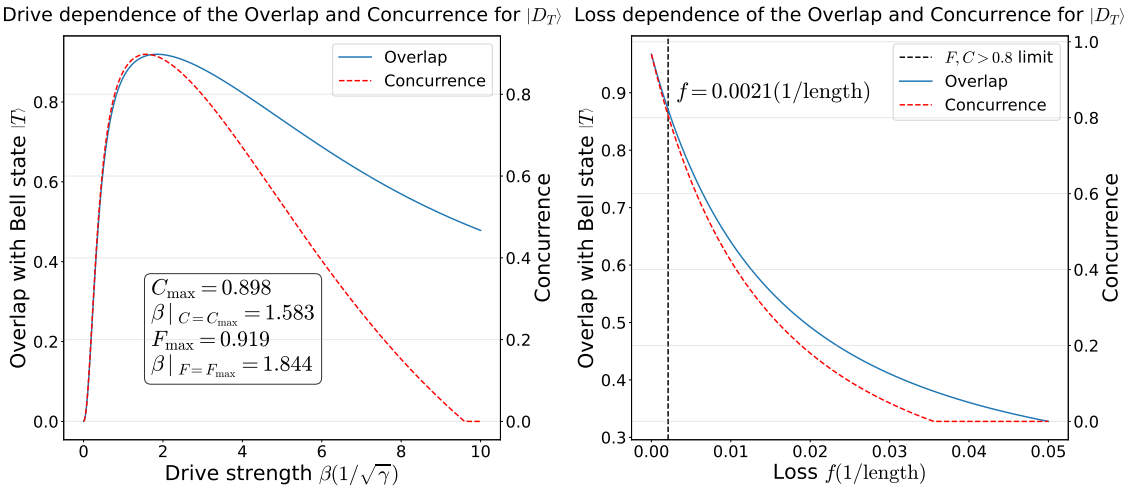

(b) Parameters: $d_T = 2\lambda + \lambda/2$. Depending on the variable, we fix $f_{\text{fixed}} = 0.001(1/\text{length})$ or $\beta_{\text{fixed}} = 2/\sqrt{\gamma}$.

Figure 3.5: Overlap and concurrence for states $\left|D_{S/T}\right\rangle$ of small atoms versus drive strength β attenuation coefficient f. (a) Results for state $|D_S\rangle$: With f fixed at $0.001(1/\text{length})$, the overlap peaks at $F_{\max} = 0.912$ ($\beta = 1.772/\sqrt{\gamma}$), while concurrence reaches $C_{\max} = 0.888$ ($\beta = 1.522/\sqrt{\gamma}$), with both declining thereafter. Under a fixed drive $\beta = 2/\sqrt{\gamma}$, both metrics decrease as losses increase. Both quantities exceed 0.8 provided that f is kept below $0.0018(1/\text{length})$. (b) Results for state $|D_T\rangle$: Similarly, at $f = 0.001(1/\text{length})$, the overlap and concurrence peak at $F_{\max} = 0.919$ ($\beta = 1.844/\sqrt{\gamma}$), and $C_{\max} = 0.898$ ($\beta = 1.583/\sqrt{\gamma}$), respectively. For $\beta = 2/\sqrt{\gamma}$, both values stay above 0.8 as long as $f < 0.0021(1/\text{length})$.

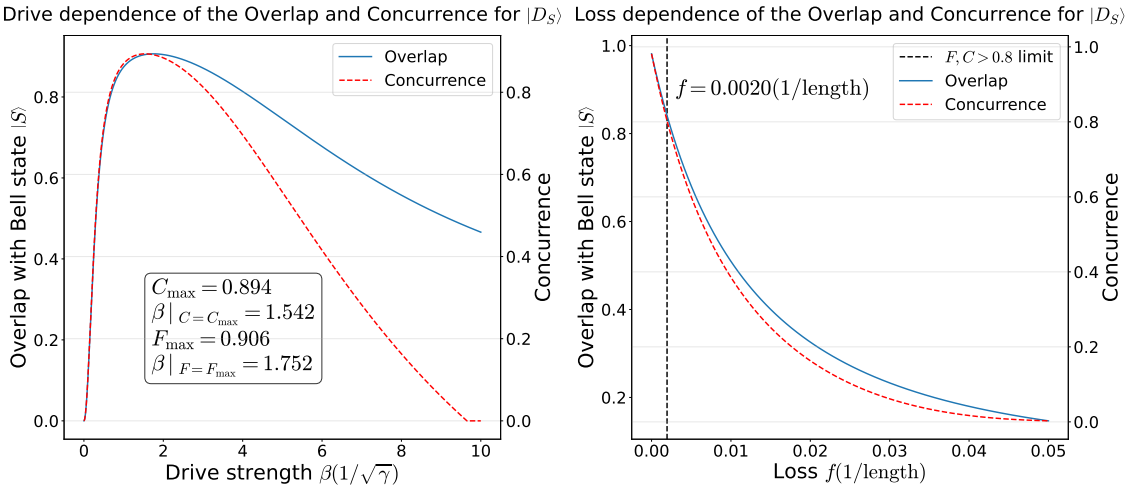

(a) Parameters: $d_{S_n} = \lambda$. Depending on the variable, we fix $f_{\text{fixed}} = 0.001(1/\text{length})$ or $\beta_{\text{fixed}} = 2/\sqrt{\gamma}$.

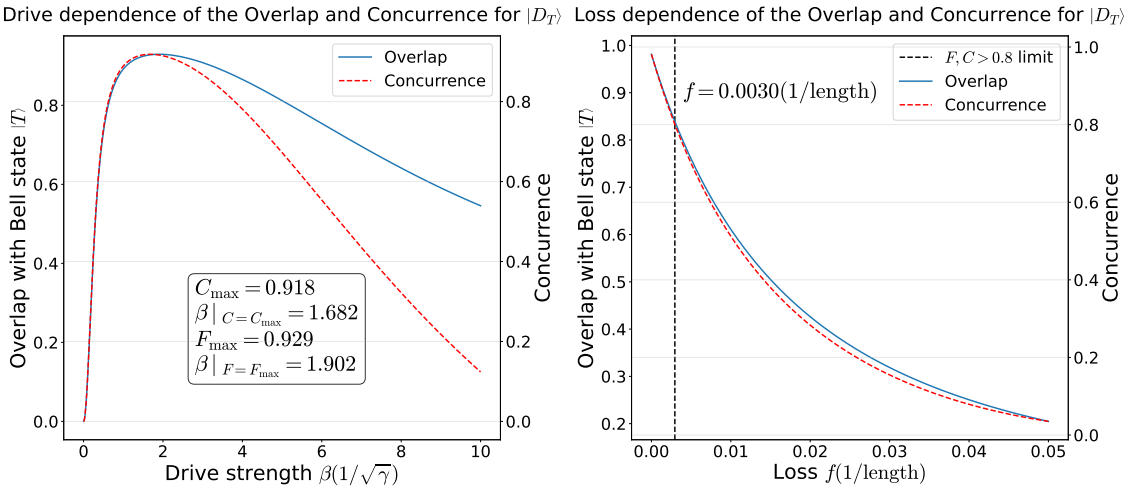

(b) Parameters: $d_{T_1} = d_{T_3} = \lambda$, $d_{T_2} = \lambda/2$. Depending on the variable, we fix $f_{\text{fixed}} = 0.001(1/\text{length})$ or $\beta_{\text{fixed}} = 2/\sqrt{\gamma}$.

Figure 3.6: Overlap and concurrence for states $\left|D_{S/T}\right\rangle$ of separate atoms versus drive strength β attenuation coefficient f. (a) Results for state $|D_S\rangle$: With f fixed at $0.001(1/\text{length})$, the overlap peaks at $F_{\max} = 0.906$ ($\beta = 1.752/\sqrt{\gamma}$), while concurrence reaches $C_{\max} = 0.894$ ($\beta = 1.542/\sqrt{\gamma}$), with both declining thereafter. Under a fixed drive $\beta = 2/\sqrt{\gamma}$, both metrics decrease as losses increase. Both quantities exceed 0.8 provided that f is kept below $0.0020(1/\text{length})$. (b) Results for state $|D_T\rangle$: Similarly, at $f = 0.001(1/\text{length})$, the overlap and concurrence peak at $F_{\max} = 0.929$ ($\beta = 1.902/\sqrt{\gamma}$), and $C_{\max} = 0.918$ ($\beta = 1.682/\sqrt{\gamma}$), respectively. For $\beta = 2/\sqrt{\gamma}$, both values stay above 0.8 as long as $f < 0.0030(1/\text{length})$.

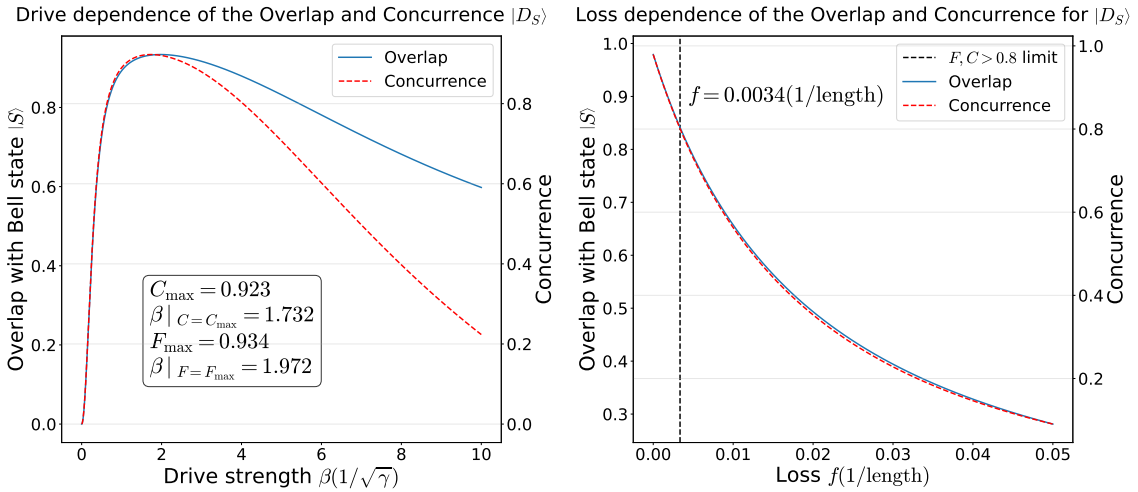

(a) Parameters: $d_{S_1} = d_{S_3} = \lambda$, $d_{S_2} = \lambda/4$. Depending on the variable, we fix $f_{\text{fixed}} = 0.001(1/\text{length})$ or $\beta_{\text{fixed}} = 2/\sqrt{\gamma}$.

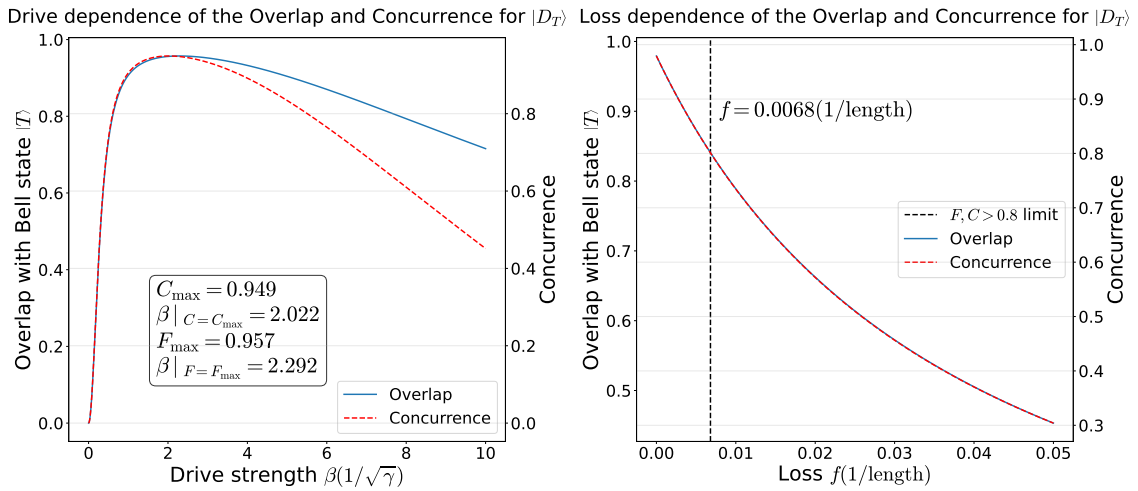

(b) Parameters: $d_{T_1} = d_{T_3} = \lambda/2$, $d_{T_2} = \lambda/4$. Depending on the variable, we fix $f_{\text{fixed}} = 0.001(1/\text{length})$ or $\beta_{\text{fixed}} = 2/\sqrt{\gamma}$.

Figure 3.7: Overlap and concurrence for states $\left|D_{S/T}\right\rangle$ of braided atoms versus drive strength β attenuation coefficient f. (a) Results for state $|D_S\rangle$: With f fixed at $0.001(1/\text{length})$, the overlap peaks at $F_{\max} = 0.934$ ($\beta = 1.972/\sqrt{\gamma}$), while concurrence reaches $C_{\max} = 0.923$ ($\beta = 1.732/\sqrt{\gamma}$), with both declining thereafter. Under a fixed drive $\beta = 2/\sqrt{\gamma}$, both metrics decrease as losses increase. Both quantities exceed 0.8 provided that f is kept below $0.0043(1/\text{length})$. (b) Results for state $|D_T\rangle$: Similarly, at $f = 0.001(1/\text{length})$, the overlap and concurrence peak at $F_{\max} = 0.957$ ($\beta = 2.292/\sqrt{\gamma}$), and $C_{\max} = 0.949$ ($\beta = 2.022/\sqrt{\gamma}$), respectively. For $\beta = 2/\sqrt{\gamma}$, both values stay above 0.8 as long as $f < 0.0068(1/\text{length})$.

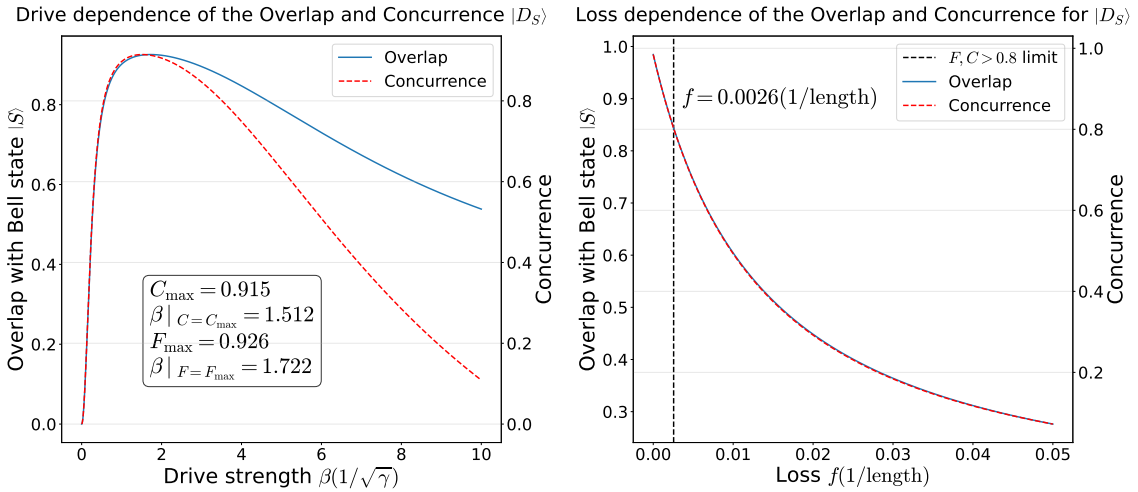

(a) Parameters: $d_{S_1} = d_{S_3} = \lambda$, $d_{S_2} = \lambda/4$. Depending on the variable, we fix $f_{\text{fixed}} = 0.001(1/\text{length})$ or $\beta_{\text{fixed}} = 2/\sqrt{\gamma}$.

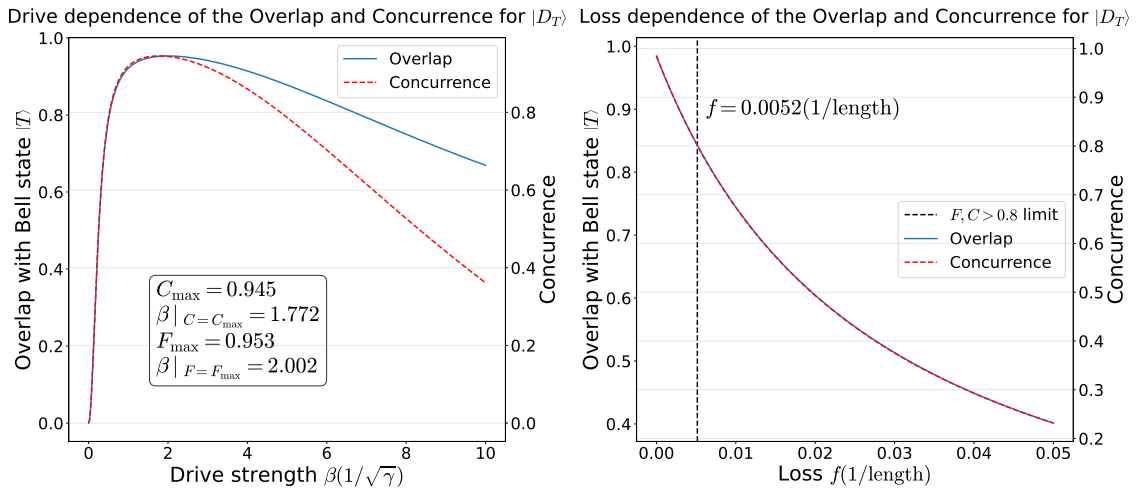

(b) Parameters: $d_{T_1} = d_{T_3} = \lambda/2$, $d_{T_2} = \lambda/4$. Depending on the variable, we fix $f_{\text{fixed}} = 0.001(1/\text{length})$ or $\beta_{\text{fixed}} = 2/\sqrt{\gamma}$.

Figure 3.8: Overlap and concurrence for states $\left|D_{S/T}\right\rangle$ of nested atoms versus drive strength β attenuation coefficient f. (a) Results for state $|D_S\rangle$: With f fixed at $0.001(1/\text{length})$, the overlap peaks at $F_{\max} = 0.926$ ($\beta = 1.722/\sqrt{\gamma}$), while concurrence reaches $C_{\max} = 0.915$ ($\beta = 1.512/\sqrt{\gamma}$), with both declining thereafter. Under a fixed drive $\beta = 2/\sqrt{\gamma}$, both metrics decrease as losses increase. Both quantities exceed 0.8 provided that f is kept below $0.0026(1/\text{length})$. (b) Results for state $|D_T\rangle$: Similarly, at $f = 0.001(1/\text{length})$, the overlap and concurrence peak at $F_{\max} = 0.953$ ($\beta = 2.002/\sqrt{\gamma}$), and $C_{\max} = 0.945$ ($\beta = 1.772/\sqrt{\gamma}$), respectively. For $\beta = 2/\sqrt{\gamma}$, both values stay above 0.8 as long as $f < 0.0052(1/\text{length})$.

4

Conclusions and Outlook

In this thesis, we investigate two major imperfections in giant-atom systems that degrade the mechanisms of decoherence suppression. Specifically, asymmetric coupling destroys the self-interference effect, resulting in a non-zero relaxation rate at frequencies that previously were completely protected from relaxation. As a consequence, decoherence-free interaction can no longer be perfectly achieved, which is consistent with physical intuition. In this thesis, asymmetric coupling refers to the situation where the bare relaxation rates at coupling points belonging to the same atom are unequal. It should also be emphasized that this work does not provide a detailed and deep discussion of the symmetric couplings for dark-state formation. In Sec. 2.3.3.2 and Table B.1, the discussion is based on the assumption that $\gamma_{nR/L} = \gamma_{R/L}$. Under this assumption, the nested configuration can still support dark states even in the presence of asymmetric left- and right-propagation couplings ($\gamma_R \neq \gamma_L$), owing to the geometry-induced internal interference of the nested configuration. However, this is not generally valid in the asymmetric coupling cases in which the bare relaxation rates are unequal from the same atom, where symmetric left- and right-propagating couplings ($\gamma_R = \gamma_L$) are required in order to satisfy $g \in \mathbb{R}$.

Besides asymmetric coupling, another practically unavoidable imperfection is photon loss in the waveguide. Such losses introduce a non-zero minimum relaxation rate; not only is this minimum no longer zero, but the topology required to achieve it also shifts away from a half-wavelength distance between neighboring coupling points. These shifts provide a useful way to identify and quantify imperfections present in realistic setups. By combining the experimental results of a single giant atom reported in Ref. [5], in which the experiment uses superconducting circuits and tunes phase shifts by changing the qubit frequencies, with our analytical expressions for the shift of the minimum relaxation rate, the upper bound of the attenuation coefficient is estimated to be approximately $0.03/\lambda$.

For dark-state formation in two-atom systems, a perfectly subradiant state cannot be maintained in the presence of losses. In the weak-loss regime and without external driving, the system gradually decays toward a ground state, while the triplet state $|T\rangle$ exhibits relatively robust entanglement during the evolution. In the driven-dissipative regime, strong drive fields should be avoided, since they significantly suppress the entanglement of the final state. Furthermore, the state $|D_T\rangle$, associated with the triplet state, demonstrates better robustness against imperfections. It

should be noted that the tolerances discussed in Sec. 3.3.2 are obtained under the specific parameter settings: drive strength $\beta = 2/\sqrt{\gamma}$, atomic detunings from the drive $\delta_a = -\delta_b = \delta = 0.05\gamma$, and the directional relaxation-rate difference $\Delta_\gamma = \gamma_L - \gamma_R = 0.3\gamma$. Different parameter choices may lead to numerically different tolerances. Nevertheless, when comparing different topological configurations under the same conditions, giant atoms generally exhibit a broader tolerance, especially for braided atoms in the state $|D_T\rangle$.

The present work mainly focuses on two giant atoms coupled to a one-dimensional waveguide. Moreover, since giant atoms exhibit geometry-dependent interference effects and enhanced robustness against imperfections, extending the analysis to multi-atom systems may reveal richer collective phenomena arising from more possible geometric topologies. Such systems might provide new opportunities for quantum state engineering and quantum simulation.

Another important direction concerns the inclusion of additional experimental imperfections beyond waveguide losses and asymmetric coupling, such as non-Markovian environmental effects [34] and imperfect emitters. Understanding how these imperfections influence decoherence suppression and entanglement generation would help bridge the gap between theoretical proposals and experimental implementations.

Finally, there is still much to be explored in the field of giant atoms due to the complexity of realistic experimental environments. The theoretical tools and models employed in this thesis, including the ideal one-dimensional waveguide [6, 33] and SLH formalism [25], have proven to be effective for analyzing giant-atom systems from a theoretical perspective. However, in practical experiments, it remains challenging to precisely control the distances between coupling points and simultaneously account for multiple sources of imperfections, which makes direct verification of the results shown in this thesis difficult. However, the result obtained in this work still provide useful insights into the robustness of different giant-atom systems and may be helpful for further experimental designs and implementations.

References

[1] T. Scheidsteger, R. Haunschild, and C. Ettl, "Historical roots and seminal papers of quantum technology 2.0," *NanoEthics*, vol. 16, no. 3, pp. 271–296, 2022.

[2] M. Elliot, S. Oscar, and M. Kathryn, "Current quantum optics research: Exploring the potential of quantum computing," *Journal of Tecnologia Quantica*, vol. 1, no. 1, pp. 30–39, 2024.

[3] A. F. Kockum, "Quantum optics with giant atoms—the first five years," in *International Symposium on Mathematics, Quantum Theory, and Cryptography*, Springer Singapore, vol. 33, 2021, pp. 125–146.

[4] J.-Q. You and F. Nori, "Atomic physics and quantum optics using superconducting circuits," *Nature*, vol. 474, no. 7353, pp. 589–597, 2011.

[5] B. Kannan et al., "Waveguide quantum electrodynamics with superconducting artificial giant atoms," *Nature*, vol. 583, no. 7818, pp. 775–779, 2020.

[6] A. Soro and A. F. Kockum, "Chiral quantum optics with giant atoms," *Physical Review A*, vol. 105, no. 2, p. 023 712, 2022.

[7] A. Frisk Kockum, P. Delsing, and G. Johansson, "Designing frequency-dependent relaxation rates and Lamb shifts for a giant artificial atom," *Physical Review A*, vol. 90, no. 1, p. 013 837, 2014.

[8] A. F. Kockum, G. Johansson, and F. Nori, "Decoherence-free interaction between giant atoms in waveguide quantum electrodynamics," *Physical Review Letters*, vol. 120, no. 14, p. 140 404, 2018.

[9] G. Chen and A. F. Kockum, "Simulating open quantum systems with giant atoms," *Quantum Science and Technology*, vol. 10, no. 2, p. 025 028, 2025.

[10] R. H. Dicke, "Coherence in spontaneous radiation processes," *Physical review*, vol. 93, no. 1, p. 99, 1954.

[11] R. Lehmberg, "Radiation from an n-atom system. ii. spontaneous emission from a pair of atoms," *Physical Review A*, vol. 2, no. 3, p. 889, 1970.

[12] G. Lenz and P. Meystre, "Resonance fluorescence from two identical atoms in a standing-wave field," *Physical Review A*, vol. 48, no. 4, p. 3365, 1993.

[13] F. Le Kien, S. D. Gupta, K. Nayak, and K Hakuta, "Nanofiber-mediated radiative transfer between two distant atoms," *Physical Review A—Atomic, Molecular, and Optical Physics*, vol. 72, no. 6, p. 063 815, 2005.

[14] P. Lodahl et al., "Chiral quantum optics," *Nature*, vol. 541, no. 7638, pp. 473–480, 2017.

[15] H. Pichler, T. Ramos, A. J. Daley, and P. Zoller, "Quantum optics of chiral spin networks," *Physical Review A*, vol. 91, no. 4, p. 042 116, 2015.
[16] K. Stannigel, P. Rabl, and P. Zoller, "Driven-dissipative preparation of entangled states in cascaded quantum-optical networks," *New Journal of Physics*, vol. 14, no. 6, p. 063 014, 2012.
[17] N. Gisin and R. Thew, "Quantum communication," *Nature photonics*, vol. 1, no. 3, pp. 165–171, 2007.
[18] C. L. Degen, F. Reinhard, and P. Cappellaro, "Quantum sensing," *Reviews of modern physics*, vol. 89, no. 3, p. 035 002, 2017.
[19] M. V. Gustafsson, T. Aref, A. F. Kockum, M. K. Ekström, G. Johansson, and P. Delsing, "Propagating phonons coupled to an artificial atom," *Science*, vol. 346, no. 6206, pp. 207–211, 2014.
[20] H.-P. Breuer and F. Petruccione, *The theory of open quantum systems*. OUP Oxford, 2002.
[21] G. Lindblad, "On the generators of quantum dynamical semigroups," *Communications in mathematical physics*, vol. 48, no. 2, pp. 119–130, 1976.
[22] A. F. Kockum, *Quantum optics with artificial atoms*. Chalmers Tekniska Hogskola (Sweden), 2014.
[23] F Bloch and A Siegert, "Magnetic resonance for nonrotating fields," *Physical Review*, vol. 57, no. 6, p. 522, 1940.
[24] G. Agarwal, "Rotating-wave approximation and spontaneous emission," *Physical Review A*, vol. 7, no. 3, p. 1195, 1973.
[25] J. Combes, J. Kerckhoff, and M. Sarovar, "The SLH framework for modeling quantum input-output networks," *Advances in Physics: X*, vol. 2, no. 3, pp. 784–888, 2017.
[26] J. Gough and M. R. James, "The series product and its application to quantum feedforward and feedback networks," *IEEE Transactions on Automatic Control*, vol. 54, no. 11, pp. 2530–2544, 2009.
[27] C. Gardiner, "Driving a quantum system with the output field from another driven quantum system," *Physical review letters*, vol. 70, no. 15, p. 2269, 1993.
[28] H. J. Carmichael, "Quantum trajectory theory for cascaded open systems," *Physical review letters*, vol. 70, no. 15, p. 2273, 1993.
[29] J. A. Kerckhoff, *Quantum Engineering with Quantum Optics*. Stanford University, 2011.
[30] P. Krantz, M. Kjaergaard, F. Yan, T. P. Orlando, S. Gustavsson, and W. D. Oliver, "A quantum engineer's guide to superconducting qubits," *Applied physics reviews*, vol. 6, no. 2, 2019.
[31] K. Lalumiere, B. C. Sanders, A. F. van Loo, A. Fedorov, A. Wallraff, and A. Blais, "Input-output theory for waveguide qed with an ensemble of inhomogeneous atoms," *arXiv preprint arXiv:1305.7135*, 2013.
[32] P.-O. Guimond, H. Pichler, A. Rauschenbeutel, and P. Zoller, "Chiral quantum optics with v-level atoms and coherent quantum feedback," *Physical Review A*, vol. 94, no. 3, p. 033 829, 2016.
[33] A. S. Àlvarez, *Preventing Decoherence with Giant Atoms*. Chalmers University of Technology, 2025.

[34] G. Andersson, B. Suri, L. Guo, T. Aref, and P. Delsing, "Non-exponential decay of a giant artificial atom," *Nature Physics*, vol. 15, no. 11, pp. 1123–1127, 2019.

A

Coherently driven system

Using the SLH formalism, the master equation for the system coupled to an ideal waveguide can be written as

$$\dot{\rho}_1 = -i[H_u + H_{\text{drive}}, \rho] + \mathcal{D}[L_R + L_d]\rho + \mathcal{D}[L_L]\rho, \tag{A.1}$$

where H_{drive} is defined in Sec. 2.3.3.2. This master equation can be rearranged into an equivalent form:

$$\dot{\rho}_1 = -i[H_u, \rho_1] - i[H_{\text{drive}}, \rho_1] + \mathcal{D}[L_R]\rho_1 + \mathcal{D}[L_L]\rho_1 + X, \tag{A.2}$$

with

$$X = L_d\rho L_R^\dagger + L_R\rho L_d^\dagger + L_d\rho L_d^\dagger - \frac{1}{2}\left\{(L_d^\dagger L_d + L_d^\dagger L_R + L_R L_d^\dagger), \rho\right\}. \tag{A.3}$$

Substituting the relation $L_d = \beta S_R$ yields

$$X = \beta S_R\rho L_R^\dagger + L_R\rho\beta^* S_R^\dagger + |\beta|^2 S_R\rho S_R^\dagger - \frac{1}{2}\left\{(|\beta|^2 + L_R^\dagger\beta S_R + \beta^* S_R^\dagger L_R), \rho\right\}. \tag{A.4}$$

The term X is introduced so that $\dot{\rho}_1$ coincides with $\dot{\rho}$ (Eq. (2.51)).

Next we expand the combination of terms that differ in form from those in Eq. (2.51):

$$\begin{aligned} -i[H_{\text{drive}}, \rho] + X &= -\frac{1}{2}[(L_R^\dagger S_R\beta - \beta^* S_R^\dagger L_R), \rho] + X \\ &= -\beta L_R^\dagger S_R\rho - \beta^*\rho S_R^\dagger L_R + \beta S_R\rho L_R^\dagger + \beta^* L_R\rho S_R^\dagger \\ &= -i[-i(\beta S_R L_R^\dagger - \beta^* S_R^\dagger L_R), \rho] \\ &= -i[H_d, \rho]. \end{aligned} \tag{A.5}$$

Thus the dynamics described by the master equation Eq. (A.1) is identical to that described by the master equation Eq. (2.51).

In the lossy waveguide, the scattering matrices are the same for all configurations.

We therefore have

$$\begin{aligned}
\mathbf{S}_{R1} &= \begin{pmatrix} S_{R1_1} \\ S_{R1_2} \\ S_{R1_3} \\ S_{R1_4} \end{pmatrix} = \begin{pmatrix} r_{11}^1 \\ e^{i\phi_1} t_{21}^1 r_{11}^2 \\ e^{i(\phi_1+\phi_2)} t_{21}^1 t_{21}^2 r_{11}^3 \\ e^{i(\phi_1+\phi_2+\phi_3)} t_{21}^1 t_{21}^2 t_{21}^3 \end{pmatrix}, \\
\mathbf{S}_{R2} &= \begin{pmatrix} t_{12}^1 \\ e^{i\phi_1} r_{22}^1 r_{11}^2 \\ e^{i(\phi_1+\phi_2)} r_{22}^1 t_{21}^2 r_{11}^3 \\ e^{i(\phi_1+\phi_2+\phi_3)} r_{22}^1 t_{21}^2 t_{21}^3 \end{pmatrix}, \\
\mathbf{S}_{R3} &= \begin{pmatrix} 0 \\ t_{12}^2 \\ e^{i\phi_2} r_{22}^2 r_{11}^3 \\ e^{i(\phi_2+\phi_3)} r_{22}^2 t_{21}^3 \end{pmatrix}, \\
\mathbf{S}_{R4} &= \begin{pmatrix} 0 \\ 0 \\ t_{12}^3 \\ e^{i\phi_3} r_{22}^3 \end{pmatrix}.
\end{aligned} \tag{A.6}$$

The vector of jump operators that includes the driven term is

$$\mathbf{L}_d\Big|_{\text{loss}} = \begin{pmatrix} L_{d1} \\ L_{d2} \\ L_{d3} \\ L_{d4} \end{pmatrix} = \begin{pmatrix} \beta r_{11}^1 \\ e^{i\phi_1} \beta t_{21}^1 \\ e^{i(\phi_1+\phi_2)} \beta t_{21}^1 t_{21}^2 r_{11}^3 \\ e^{i(\phi_1+\phi_2+\phi_3)} \beta t_{21}^1 t_{21}^2 t_{21}^3 \end{pmatrix}. \tag{A.7}$$

For each component i, we define

$$\begin{aligned}
X_i &= L_{di}\rho L_{Ri}^\dagger + L_{Ri}\rho L_{di}^\dagger + L_{di}\rho L_{di}^\dagger - \frac{1}{2}\left\{(L_{di}^\dagger L_{di} + L_{di}^\dagger L_{Ri} + L_{Ri} L_{di}^\dagger), \rho\right\} \\
&= \beta S_{R1_i}\rho L_{Ri}^\dagger + L_{Ri}\rho\beta^* S_{R1_i}^\dagger + |\beta|^2 S_{R1_i}\rho S_{R1_i}^\dagger \\
&\quad - \frac{1}{2}\left\{(|\beta|^2 + L_{Ri}^\dagger \beta S_{R1_i} + \beta^* S_{R1_i}^\dagger L_{Ri}), \rho\right\}.
\end{aligned} \tag{A.8}$$

Then we take the sum over all components $X = \sum_i^4 X_i$. By applying the same steps as in the ideal-waveguide case, one can show that the master equation Eq. (2.51) also correctly describes the dynamics of the atoms coupled to the lossy waveguide.

B

Summary of the constraints on the dark states in the ideal waveguide

Here, we show the constraints of forming dark states in the driven and undriven systems in two tables. We only consider two-atom systems coupled to an ideal waveguide.

B.1 Undriven system

Table B.1: Constraints on phase shifts and bare relaxation rates for the formation of dark states. We set phase shifts ϕ_n and assume equal bare relaxation rates at each coupling point, $\gamma_{nR} = \gamma_R$, $\gamma_{nL} = \gamma_L$. The derivation further requires equal atomic frequencies, $\omega_a = \omega_b$, and real exchange interactions, $g = g^* \in \mathbb{R}$. Adapted from Ref. [6].

Topologies	Dark states	Phase shifts	Bare relaxation rates
Small	$\|S\rangle$	$\phi_1 = 0$	$\gamma_{nR} = \gamma_{nL} = \gamma$
	$\|T\rangle$	$\phi_1 = \pi$	$\gamma_{nR} = \gamma_{nL} = \gamma$
Separate	$\|S\rangle$	$\phi_1 = \phi_3 \neq \pi$	$\gamma_{nR} = \gamma_{nL} = \gamma$
		$\phi_1 = -\phi_2$	
	$\|T\rangle$	$\phi_1 = \phi_3 \neq \pi$	$\gamma_{nR} = \gamma_{nL} = \gamma$
		$\phi_1 + \phi_2 = \pi$	
Braided	$\|S\rangle$	$\phi_1 = \phi_3 = 0$	$\gamma_{nR} = \gamma_{nL} = \gamma$
		$\phi_2 \neq \pi$	
	$\|T\rangle$	$\phi_1 = \phi_3 = \pi$	$\gamma_{nR} = \gamma_{nL} = \gamma$
		$\phi_2 \neq 0$	
Nested	$\|S\rangle$	$\phi_1 = \phi_3 = 0$	Any
		$\phi_2 \neq \pi$	

Continued on next page

Table B.1 – continued from previous page

Topologies	Dark States	Phase shits	Bare relaxation rates
	$\|T\rangle$	$\phi_1 = \phi_3 = \pi$ $\phi_2 \neq \pi$	Any

B.2 Coherently driven system

Table B.2: Constraints on phase shifts and functions of α for dark states in the driven system. We also set phase shifts, ϕ_n and assume equal bare relaxation rates at each coupling point, $\gamma_{nR} = \gamma_R$, $\gamma_{nL} = \gamma_L$. Besides, in order to forming the dark states, some detunings should satisfy: $\Delta_\gamma = \gamma_L - \gamma_R$, $\delta = \delta_a = -\delta_b$. Adapted from Ref. [6].

Topologies	Dark states	Phase shifts	$\alpha(\beta)$
Small	$\|D_S\rangle$	$\phi_1 = 0$	$\frac{2\sqrt{2}\beta\sqrt{\gamma_R}}{\Delta_\gamma - 2i\delta}$
	$\|D_T\rangle$	$\phi_1 = \pi$	$\frac{2\sqrt{2}\beta\sqrt{\gamma_R}}{\Delta_\gamma - 2i\delta}$
Separate	$\|D_S\rangle$	$\phi_1 = \phi_2 = \phi_3 = 0$	$\frac{2\sqrt{2}\beta\sqrt{\gamma_R}}{2\Delta_\gamma - i\delta}$
	$\|D_T\rangle$	$\phi_1 = \phi_3 = 0$ $\phi_2 = \pi$	$\frac{2\sqrt{2}\beta\sqrt{\gamma_R}}{2\Delta_\gamma - i\delta}$
Braided	$\|D_S\rangle$	$\phi_1 = \phi_3 = 0$ $\phi_2 \neq \pi$	$\frac{\sqrt{2}\beta\sqrt{\gamma_R}(1+e^{i\phi_2})}{\Delta_\gamma - i\delta}$
	$\|D_T\rangle$	$\phi_1 = \phi_3 = \pi$ $\phi_2 \neq 0$	$\frac{\sqrt{2}\beta\sqrt{\gamma_R}(1-e^{i\phi_2})}{\Delta_\gamma - i\delta}$
Nested	$\|D_S\rangle$	$\phi_1 = \phi_3 = 0$	$\frac{\sqrt{2}\beta\sqrt{\gamma_R}(1+e^{i\phi_2})}{-i\delta}$

Continued on next page

Table B.2 – continued from previous page

Topologies	Dark States	Phase shits	Bare relaxation rates
	$\|D_T\rangle$	$\phi_2 \neq \pi$ $\phi_1 = \phi_3 = \pi$ $\phi_2 \neq \pi$	$\frac{\sqrt{2}\beta\sqrt{\gamma_R}(1+e^{i\phi_2})}{-i\delta}$

C

Results for the atoms coupled to a lossy waveguide

In this section, we show the general results for two-atom systems coupled to a lossy waveguide, including frequency shifts, individual and collective relaxation rates, and exchange interactions.

Table C.1: Frequency shifts δ_{ω_j} for small and giant atoms coupled to a lossy waveguide. We assume arbitrary bare relaxation rates $\gamma_{nR/L}$ at each coupling point $n = 1, 2, 3, 4$, beam splitter transmission coefficients t_{12}^n and t_{21}^n, and phase shifts ϕ_n between adjacent coupling points.

Topologies	**Frequency shifts**
Small	$\delta_{\omega_a} = 0$ $\delta_{\omega_b} = 0$
Separate	$\delta_{\omega_a} = \frac{1}{2i}\Big[\sqrt{\gamma_{1R}\gamma_{2R}}\left(t_{21}^{1}e^{i\phi_1} - t_{21}^{1*}e^{-i\phi_1}\right)$ $+\sqrt{\gamma_{1L}\gamma_{2L}}\left(t_{12}^{1}e^{i\phi_1} - t_{12}^{1*}e^{-i\phi_1}\right)\Big]$ $\delta_{\omega_b} = \frac{1}{2i}\Big[\sqrt{\gamma_{3R}\gamma_{4R}}\left(t_{21}^{3}e^{i\phi_3} - t_{21}^{3*}e^{-i\phi_3}\right)$ $+\sqrt{\gamma_{3L}\gamma_{4L}}\left(t_{12}^{3}e^{i\phi_3} - t_{12}^{3*}e^{-i\phi_3}\right)\Big]$

Continued on next page

Table C.1 – continued from previous page

Topologies	Frequency shifts
Braided	$\delta_{\omega_a} = \frac{1}{2i}\Big[\sqrt{\gamma_{1R}\gamma_{3R}}\left(t_{21}^{1}t_{21}^{2}e^{i(\phi_1+\phi_2)} - t_{21}^{1*}t_{21}^{2*}e^{-i(\phi_1+\phi_2)}\right) + \sqrt{\gamma_{1L}\gamma_{3L}}\left(t_{12}^{1}t_{12}^{2}e^{i(\phi_1+\phi_2)} - t_{12}^{1*}t_{12}^{2*}e^{-i(\phi_1+\phi_2)}\right)\Big]$ $\delta_{\omega_b} = \frac{1}{2i}\Big[\sqrt{\gamma_{2R}\gamma_{4R}}\left(t_{21}^{2}t_{21}^{3}e^{i(\phi_2+\phi_3)} - t_{21}^{2*}t_{21}^{3*}e^{-i(\phi_2+\phi_3)}\right) + \sqrt{\gamma_{2L}\gamma_{4L}}\left(t_{12}^{2}t_{12}^{3}e^{i(\phi_2+\phi_3)} - t_{12}^{2*}t_{12}^{3*}e^{-i(\phi_2+\phi_3)}\right)\Big]$
Nested	$\delta_{\omega_a} = \frac{1}{2i}\Big[\sqrt{\gamma_{1R}\gamma_{4R}}\left(t_{21}^{1}t_{21}^{2}t_{21}^{3}e^{i(\phi_1+\phi_2+\phi_3)} - t_{21}^{1*}t_{21}^{2*}t_{21}^{3*}e^{-i(\phi_1+\phi_2+\phi_3)}\right) + \sqrt{\gamma_{1L}\gamma_{4L}}\left(t_{12}^{1}t_{12}^{2}t_{12}^{3}e^{i(\phi_1+\phi_2+\phi_3)} - t_{12}^{1*}t_{12}^{2*}t_{12}^{3*}e^{-i(\phi_1+\phi_2+\phi_3)}\right)\Big]$ $\delta_{\omega_b} = \frac{1}{2i}\Big[\sqrt{\gamma_{2R}\gamma_{3R}}\left(t_{21}^{2}e^{i\phi_2} - t_{21}^{2*}e^{-i\phi_2}\right) + \sqrt{\gamma_{2L}\gamma_{3L}}\left(t_{12}^{2}e^{i\phi_2} - t_{12}^{2*}e^{-i\phi_2}\right)\Big]$

Table C.2: Individual relaxation rates Γ_j for small and giant atoms, with the same setups in Table. C.1.

Topologies	Individual relaxation rates
Small	$\Gamma_a = \gamma_{1R} + \gamma_{1L}$ $\Gamma_b = \gamma_{2R} + \gamma_{2L}$
Separate	$\Gamma_a = \gamma_{1R} + \gamma_{2R} + \gamma_{1L} + \gamma_{2L} + \sqrt{\gamma_{1R}\gamma_{2R}}(t_{21}^{1}e^{i\phi_1} + t_{21}^{1*}e^{-i\phi_1}) + \sqrt{\gamma_{1L}\gamma_{2L}}(t_{12}^{1}e^{i\phi_1} + t_{12}^{1*}e^{-i\phi_1})$ $\Gamma_b = \gamma_{3R} + \gamma_{4R} + \gamma_{3L} + \gamma_{4L} + \sqrt{\gamma_{3R}\gamma_{4R}}(t_{21}^{3}e^{i\phi_3} + t_{21}^{3*}e^{-i\phi_3}) + \sqrt{\gamma_{3L}\gamma_{4L}}(t_{12}^{3}e^{i\phi_3} + t_{12}^{3*}e^{-i\phi_3})$

Continued on next page

Table C.2 – continued from previous page

Topologies	Individual relaxation rates
Braided	$\Gamma_a = \gamma_{1R} + \gamma_{3R} + \gamma_{1L} + \gamma_{3L}$ $+ \sqrt{\gamma_{1R}\gamma_{3R}}(t_{21}^1 t_{21}^2 e^{i(\phi_1+\phi_2)} + t_{21}^{1*} t_{21}^{2*} e^{-i(\phi_1+\phi_2)})$ $+ \sqrt{\gamma_{1L}\gamma_{3L}}(t_{12}^1 t_{12}^2 e^{i(\phi_1+\phi_2)} + t_{12}^{1*} t_{12}^{2*} e^{-i(\phi_1+\phi_2)})$ $\Gamma_b = \gamma_{2R} + \gamma_{4R} + \gamma_{2L} + \gamma_{4L}$ $+ \sqrt{\gamma_{2R}\gamma_{4R}}(t_{21}^2 t_{21}^3 e^{i(\phi_2+\phi_3)} + t_{21}^{2*} t_{21}^{3*} e^{-i(\phi_2+\phi_3)})$ $+ \sqrt{\gamma_{2L}\gamma_{4L}}(t_{12}^2 t_{12}^3 e^{i(\phi_2+\phi_3)} + t_{12}^{2*} t_{12}^{3*} e^{-i(\phi_2+\phi_3)})$
Nested	$\Gamma_a = \gamma_{1R} + \gamma_{4R} + \gamma_{1L} + \gamma_{4L}$ $+ \sqrt{\gamma_{1R}\gamma_{4R}}(t_{21}^1 t_{21}^2 t_{21}^3 e^{i(\phi_1+\phi_2+\phi_3)} + t_{21}^{1*} t_{21}^{2*} t_{21}^{3*} e^{-i(\phi_1+\phi_2+\phi_3)})$ $+ \sqrt{\gamma_{1L}\gamma_{4L}}(t_{12}^1 t_{12}^2 t_{12}^3 e^{i(\phi_1+\phi_2+\phi_3)} + t_{12}^{1*} t_{12}^{2*} t_{12}^{3*} e^{-i(\phi_1+\phi_2+\phi_3)})$ $\Gamma_b = \gamma_{2R} + \gamma_{3R} + \gamma_{2L} + \gamma_{3L}$ $+ \sqrt{\gamma_{2R}\gamma_{3R}}(t_{21}^2 e^{i\phi_2} + t_{21}^{2*} e^{-i\phi_2}) + \sqrt{\gamma_{2L}\gamma_{3L}}(t_{12}^2 e^{i\phi_2} + t_{12}^{2*} e^{-i\phi_2})$

Table C.3: Collective relaxation rates Γ_{coll} for small and giant atoms, with the same setups in Table. C.1.

Topologies	Collective relaxation rates
Small	$\Gamma_{\text{coll}} = e^{i\phi_1} t_{21}^1 \sqrt{\gamma_{1R}\gamma_{2R}} + e^{-i\phi_1} t_{12}^{1*} \sqrt{\gamma_{1L}\gamma_{2L}}$
Separate	$\Gamma_{\text{coll}} = \sqrt{\gamma_{1R}\gamma_{3R}} t_{21}^1 t_{21}^2 e^{i(\phi_1+\phi_2)} + \sqrt{\gamma_{2R}\gamma_{3R}} t_{21}^2 e^{i\phi_2}$ $+ \sqrt{\gamma_{1R}\gamma_{4R}} t_{21}^3 t_{21}^2 t_{21}^1 e^{i(\phi_1+\phi_2+\phi_3)} + \sqrt{\gamma_{2R}\gamma_{4R}} t_{21}^3 t_{21}^2 e^{i(\phi_2+\phi_3)}$ $+ \sqrt{\gamma_{1L}\gamma_{3L}} t_{12}^{1*} t_{12}^{2*} e^{-i(\phi_1+\phi_2)} + \sqrt{\gamma_{2L}\gamma_{3L}} t_{12}^{2*} e^{-i\phi_2}$ $+ \sqrt{\gamma_{1L}\gamma_{4L}} t_{12}^{3*} t_{12}^{2*} t_{12}^{1*} e^{-i(\phi_1+\phi_2+\phi_3)} + \sqrt{\gamma_{2L}\gamma_{4L}} t_{12}^{3*} t_{12}^{2*} e^{-i(\phi_2+\phi_3)}$
Braided	$\Gamma_{\text{coll}} = \sqrt{\gamma_{1R}\gamma_{2R}} t_{21}^1 e^{i\phi_1} + \sqrt{\gamma_{1R}\gamma_{4R}} t_{21}^1 t_{21}^2 t_{21}^3 e^{i(\phi_1+\phi_2+\phi_3)}$ $+ \sqrt{\gamma_{2R}\gamma_{3R}} t_{21}^{2*} e^{-i\phi_2} + \sqrt{\gamma_{3R}\gamma_{4R}} t_{21}^3 e^{i\phi_3}$ $+ \sqrt{\gamma_{1L}\gamma_{2L}} t_{12}^{1*} e^{-i\phi_1} + \sqrt{\gamma_{1L}\gamma_{4L}} t_{12}^{1*} t_{12}^{2*} t_{12}^{3*} e^{-i(\phi_1+\phi_2+\phi_3)}$ $+ \sqrt{\gamma_{2L}\gamma_{3L}} t_{12}^2 e^{i\phi_2} + \sqrt{\gamma_{3L}\gamma_{4L}} t_{12}^{3*} e^{-i\phi_3}$

Continued on next page

Table C.3 – continued from previous page

Topologies	Collective relaxation rates
Nested	$\Gamma_{\text{coll}} = \sqrt{\gamma_{1R}\gamma_{2R}}t_{21}^{1}e^{i\phi_1} + \sqrt{\gamma_{1R}\gamma_{3R}}t_{21}^{1}t_{21}^{2}e^{i(\phi_1+\phi_2)} + \sqrt{\gamma_{2R}\gamma_{4R}}t_{21}^{2*}t_{21}^{3*}e^{-i(\phi_2+\phi_3)} + \sqrt{\gamma_{3R}\gamma_{4R}}t_{21}^{3*}e^{-i\phi_3} + \sqrt{\gamma_{1L}\gamma_{2L}}t_{12}^{1*}e^{-i\phi_1} + \sqrt{\gamma_{1L}\gamma_{3L}}t_{12}^{1*}t_{12}^{2*}e^{-i(\phi_1+\phi_2)} + \sqrt{\gamma_{2L}\gamma_{4L}}t_{12}^{2}t_{12}^{3}e^{i(\phi_2+\phi_3)} + \sqrt{\gamma_{3L}\gamma_{4L}}t_{12}^{3}e^{i\phi_3}$

Table C.4: Exchange interactions g for small and giant atoms, with the same setups in Table. C.1.

Topologies	Exchange interactions
Small	$g = \frac{1}{2i}\left(\sqrt{\gamma_{1R}\gamma_{2R}}t_{21}^{1}e^{i\phi_1} - \sqrt{\gamma_{1L}\gamma_{2L}}t_{12}^{1*}e^{-i\phi_1}\right)$
Separate	$g = \frac{1}{2i}\Big[\sqrt{\gamma_{1R}\gamma_{3R}}t_{21}^{1}t_{21}^{2}e^{i(\phi_1+\phi_2)} + \sqrt{\gamma_{2R}\gamma_{3R}}t_{21}^{2}e^{i\phi_2} + \sqrt{\gamma_{2R}\gamma_{4R}}t_{21}^{2}t_{21}^{3}e^{i(\phi_2+\phi_3)} + \sqrt{\gamma_{1R}\gamma_{4R}}t_{21}^{3}t_{21}^{2}t_{21}^{1}e^{i(\phi_1+\phi_2+\phi_3)} - \sqrt{\gamma_{1L}\gamma_{3L}}t_{12}^{1*}t_{12}^{2*}e^{-i(\phi_1+\phi_2)} - \sqrt{\gamma_{2L}\gamma_{3L}}t_{12}^{2*}e^{-i\phi_2} - \sqrt{\gamma_{2L}\gamma_{4L}}t_{12}^{2*}t_{12}^{3*}e^{-i(\phi_2+\phi_3)} - \sqrt{\gamma_{1L}\gamma_{4L}}t_{12}^{1*}t_{12}^{2*}t_{12}^{3*}e^{-i(\phi_1+\phi_2+\phi_3)}\Big]$
Braided	$g = \frac{1}{2i}\Big[\sqrt{\gamma_{1R}\gamma_{2R}}t_{21}^{1}e^{i\phi_1} + \sqrt{\gamma_{3R}\gamma_{4R}}t_{21}^{3}e^{i\phi_3} + \sqrt{\gamma_{1R}\gamma_{4R}}t_{21}^{1}t_{21}^{2}t_{21}^{3}e^{i(\phi_1+\phi_2+\phi_3)} - \sqrt{\gamma_{2R}\gamma_{3R}}t_{21}^{2*}e^{-i\phi_2} - \sqrt{\gamma_{1L}\gamma_{2L}}t_{12}^{1*}e^{-i\phi_1} - \sqrt{\gamma_{3L}\gamma_{4L}}t_{12}^{3*}e^{-i\phi_3} - \sqrt{\gamma_{1L}\gamma_{4L}}t_{12}^{1*}t_{12}^{2*}t_{12}^{3*}e^{-i(\phi_1+\phi_2+\phi_3)} + \sqrt{\gamma_{2L}\gamma_{3L}}t_{12}^{2}e^{i\phi_2}\Big]$
Nested	$g = \frac{1}{2i}\Big[\sqrt{\gamma_{1R}\gamma_{2R}}t_{21}^{1}e^{i\phi_1} + \sqrt{\gamma_{1R}\gamma_{3R}}t_{21}^{1}t_{21}^{2}e^{i(\phi_1+\phi_2)} - \sqrt{\gamma_{3R}\gamma_{4R}}t_{21}^{3*}e^{-i\phi_3} - \sqrt{\gamma_{2R}\gamma_{4R}}t_{21}^{2*}t_{21}^{3*}e^{-i(\phi_2+\phi_3)} - \sqrt{\gamma_{1L}\gamma_{2L}}t_{12}^{1*}e^{-i\phi_1} - \sqrt{\gamma_{1L}\gamma_{3L}}t_{12}^{1*}t_{12}^{2*}e^{-i(\phi_1+\phi_2)} + \sqrt{\gamma_{3L}\gamma_{4L}}t_{12}^{3}e^{i\phi_3} + \sqrt{\gamma_{2L}\gamma_{4L}}t_{12}^{2}t_{12}^{3}e^{i(\phi_2+\phi_3)}\Big]$

DEPARTMENT OF MICROTECHNOLOGY AND NANOSCIENCE
CHALMERS UNIVERSITY OF TECHNOLOGY
Gothenburg, Sweden
www.chalmers.se

CHALMERS
UNIVERSITY OF TECHNOLOGY